√ FDL-TDR-64-144

# PRESSURE AND HEAT TRANSFER MEASUREMENTS AT MACH 13 AND 19 FOR FLOWS AHEAD OF RAMPS, OVER EXPANSION CORNERS, AND PAST FIN-PLATE COMBINATIONS

## PART OF AN INVESTIGATION OF HYPERSONIC FLOW SEPARATION AND CONTROL CHARACTERISTICS

TECHNICAL DOCUMENTARY REPORT No. FDL-TDR-64-144

SEPTEMBER 1964

AIR FORCE FLIGHT DYNAMICS LABORATORY
RESEARCH AND TECHNOLOGY DIVISION
AIR FORCE SYSTEMS COMMAND
WRIGHT-PATTERSON AIR FORCE BASE, OHIO

# NOTICES

Qualified requesters may obtain copies of this report from the Defense Documentation Center (DDC), (formerly ASTIA), Cameron Station, Bldg. 5, 5010 Duke Street, Alexandria, Virginia, 22314.

This report has been released to the Office of Technical Services, U.S. Department of Commerce, Washington 25, D. C., in stock quantities for sale to the general public.

Copies of this report should not be returned to the Research and Technology Division, Wright-Patterson Air Force Base, Ohio, unless return is required by security considerations, contractual obligations, or notice on a specific document.

SCO - November 1964 - 448-11-313

## FOREWORD

This report presents the results of a portion of the experimental program for an investigation of hypersonic flow separation and control characteristics conducted by the Research Department of Grumman Aircraft Engineering Corporation, Bethpage, New York. The work was partly sponsored by the Flight Dynamics Laboratory, Research and Technology Division, Wright-Patterson Air Force Base, Ohio, under Contract AF33(616)-8130, Air Force Task 821902. Mr. Donald E. Hoak was the Air Force Project Engineer for the program.

## ABSTRACT

This report presents heat transfer and pressure distributions for hypersonic flows ahead of ramps, over expansion corners, and past fin-plate combinations. Two basic models were used for these experiments: 1) a flat plate with a full span ramp (trailing-edge flap) on one surface and an expansion corner on the other, and 2) a flat plate with wedge shaped fins mounted on the upper surface and an expansion corner on the lower surface. Both sharp leading edge models were tested in the Grumman Hypersonic Shock Tunnel at Mach 13 and 19. The plate-flap model was tested at $\alpha = -15°$ to $+30°$, with flap deflections from $0°$ to $45°$, at Reynolds numbers per foot of $0.8 \times 10^5$ to $1.4 \times 10^5$ at Mach 19 and of $1.2 \times 10^5$ at Mach 13. The fin-plate model was tested at $\alpha = 0$ only, with 15 degree wedge shaped fins having two different heights at a Reynolds number per foot of $2.4 \times 10^5$ at Mach 13 and of $0.8 \times 10^5$ at Mach 19.

This technical documentary report has been reviewed and is approved.

for *C. R. Bryan*

W. A. SLOAN, Jr.
Colonel, USAF
Chief, Flight Control Division
AF Flight Dynamics Laboratory

iii

# TABLE OF CONTENTS

LIST OF ILLUSTRATIONS

LIST OF ILLUSTRATIONS (Cont)

vi

## LIST OF ILLUSTRATIONS (Cont)

# LIST OF TABLES

## LIST OF SYMBOLS

$C_p$      pressure coefficient, $C_p \equiv (p - p_\infty)/q_\infty$

h      heat transfer coefficient (BTU/ft$^2$ sec °R),
$h \equiv \dot{q}_w/(T_o - T_w)$

$k_\infty$      thermal conductivity of free stream flow (BTU/ft sec °R)[*]

$M_\infty$      free stream Mach number[*]

Nu      Nusselt number, $Nu \equiv hx/k_\infty$

p      pressure (psia)

$P_o$      stagnation pressure (psia)

$p_\infty$      free stream static pressure (psia)[*]

$\dot{q}_w$      aerodynamic heating rate (BTU/ft$^2$ sec)

$q_\infty$      free stream dynamic pressure (psia)[*]

$Re_x$      local Reynolds number $Re_x \equiv \rho_\infty U_\infty x/\mu_\infty$

$Re_\infty/ft$      free stream Reynolds number per foot, $Re_\infty/ft \equiv \rho_\infty U_\infty/\mu_\infty$[*]

S      nondimensional streamwise distance

$S_u$      upper surface streamwise distance

$S_\ell$      lower surface streamwise distance

t      time (sec)

$T_o$      stagnation temperature (°R)

$T_w$          wall temperature  (°R)

$T_\infty$          free stream static temperature  (°R)[*]

$U_\infty$          free stream velocity (ft/sec)[*]

x, y, z   coordinate axes defined in Figs. 2 and 4

$\mu_\infty$          free stream viscosity (slugs/ft sec)

$\rho_\infty$          free stream density (slugs/ft$^3$).

[*]Free stream properties are calculated at the leading edge
model station.

# INTRODUCTION

The Grumman Research Department has been investigating hypersonic flow separation and the effectiveness of controls in separated flow zones. The experimental effort involved testing four basic configurations in the Arnold Engineering Development Center (AEDC) Tunnels A, B, and Hotshot 2, as well as in the Grumman Hypersonic Shock Tunnel (GHST). Eleven distinct models were built in order to accommodate pressure, heat transfer, and force measurements as well as to meet the requirements of the various facilities. Sketches of the configurations, along with some pertinent remarks for the over-all program, are shown in Fig. 1. The four basic configurations are labeled A, B, C, and D. Configurations A and B were designed primarily to study flow separation, while configurations C and D were designed primarily to provide controls information for typical hypersonic flight configurations. Detailed design information and test plans are given in Ref. 1.

This report deals with configurations A and B and presents pressure and heat transfer data that were obtained in the Grumman Hypersonic Shock Tunnel at nominal Mach numbers 13 and 19 during early 1964. The models in this tunnel entry are one half scale of the ones that were tested at Mach numbers 5 and 8 at AEDC.

The purpose of the tests reported here is twofold: first to generate experimental information at Mach 13 and 19, and second to provide possible guidelines for extending the Mach 5 and 8 data to higher Mach numbers. Results for the over-all program will be presented in a forthcoming final report. Two runs were made using Krylon white enamel as a heat sensitive paint and the results are discussed briefly. Schlieren photography was employed and some typical photographs are presented.

---------------

1

## MODELS

Dimensions, pressure tap, and thermocouple locations as
well as coordinate axes definitions for model A are given in
Fig. 2. Instrumentation coordinates are given in Table I.
Model A has a six-inch square planform and a nominally sharp
leading edge (35° included angle). The upper surface was de-
signed for the study of the flow ahead of ramps and the lower
surface for the study of the flow over 40° expansion corners.
The trailing edge flap is of 25 per cent chord and is shown in
Fig. 2 for the three flap settings studied in this tunnel entry.

Model B is pictured in Fig. 3; dimensions, instrumentation
locations, and coordinate axes definitions are given in Fig. 4.
Instrumentation coordinates are given in Table II. The body of
model B has a six-inch square planform with a trapezoidal
profile and is one and one half inches deep. The lower face of
the body intersects the upper surface forming an angle of 30°
at the leading edge. The leading edge of the model and the 30°
expansion corner on the lower surface are machined sharp. A
small, sharp leading edge fin is mounted symmetrically about
the centerline on the flat plate upper surface of the model.
The wedge shaped fin has a semi-vertex angle of 15°. An attach-
able fin portion provides an extra fin configuration of 2-inch height.


## TEST CONDITIONS

Model A was tested at angles of attack of -15° to +30°,
referenced to the upper flat plate surface. The convention used
here is that compression of the upper surface indicates positive
angles of attack. Model B was tested only at zero angle of
attack, also referenced to the upper flat plate surface. The
flap deflections for model A were 0, 15°, 30°, and 45°; model B
was tested with two wedge fins separately.

Both models were run at nominal Mach numbers of 13 and 19.
The range of free stream Reynolds number per foot was from 0.8 x
$10^5$ to 2.4 x $10^5$. A detailed presentation of the test program
and corresponding test conditions are shown in Table III. A
number of runs were repeated and are so indicated in the table.

The free stream conditions shown in Table III are those
obtained at the leading edge of the model. These conditions are

2

not duplicated exactly from run to run and are thus indicated in
the table. Useful test flow durations of approximately 3 milli-
seconds were obtained for these conditions. Further, because
the GHST has a conical nozzle, the free stream conditions vary
in the test section along the tunnel centerline. Distributions
of the free stream static pressure, temperature, and Mach number
along the tunnel centerline are plotted versus axial distance
downstream of the nozzle exit in Figs. 5 and 6. A more detailed
description of the facility is given in Ref. 3.

## DATA REDUCTION AND ACCURACY

Pressure and heat transfer data were reduced to the standard
coefficient forms presented herein by using reference "free stream"
conditions. These were taken as those at the leading edge of the
models.

Measured pressures $p$ were reduced to pressure coefficients,

$$C_p = \frac{p - p_\infty}{q_\infty}$$

using the reference free stream values of the static and dynamic
pressures, $p_\infty$ and $q_\infty$.

Aerodynamic heating rates $\dot{q}_w$ were presented directly by
the heat transfer gauge instruments (from measurements of the
transient wall temperatures $T_w$). The heating rates were non-
dimensionalized in the form

$$\frac{Nu}{\sqrt{Re_x}} = \left(\frac{\dot{q}_w}{T_o - T_w}\right)\left(\frac{x}{k_\infty}\right) \bigg/ \sqrt{\frac{\rho_\infty U_\infty x}{\mu_\infty}}$$

where $Nu$ is the Nusselt number, $x$ is the streamwise distance
from the leading edge to the heat transfer gauge* (see Figs. 2
and 4), and $Re_x$ is the Reynolds number based on distance $x$.

---

*For model A, $x$ is the running length at all flap settings while
for model B, $x$ is a projected length.

For each test run, the values of $k_\infty$, $\rho_\infty$, $U_\infty$, and $\mu_\infty$ (the thermal conductivity, density, velocity and viscosity of the free stream flow respectively), were calculated at the model's leading edge station. Values of $k_\infty$ and $Re_\infty/ft$ are given in Table III for each test run. For the low temperature encountered in these tests, the conductivity $k_\infty$ was calculated by assuming a Prandtl number equal to 0.73, a specific heat at constant pressure $c_p = 0.24$ BTU/lbm °R, and a viscosity depend-

ence $\mu = \dfrac{2.21\ T^{3/2}}{T + 178.6}\ \times 10^{-8}$ slugs/ft sec.

Pressures were estimated to be accurate to within 10 per cent of their measured values. In addition to these estimates, the data on the lower surface of both models provide a certain degree of repeatability, since the flow there should not be influenced by geometrical changes on the upper surface. The accuracy for the heating rates is not as good as for the pressures. This is to be expected for a facility of small duration testing time. The repeatability in most cases is good and within a 10 per cent range. In some instances, and particularly in the interaction zone of model B, repeatability of less than 10 per cent was not always obtained. This might very well be due to the sensitivity of the corner flow and not necessarily to instrumentation defects. Occasionally the oscilloscope trace of a point was very "noisy" and difficult to read. Such points have been omitted in the presentation of the data. Lastly, we mention that artificial errors may be introduced in the process of nondimensionalizing the data, since the free stream conditions can very well vary.


PRESENTATION OF RESULTS


The presentation of the data differs distinctly for the two models. For model A the pressure and heat transfer rates are plotted versus a nondimensionalized streamwise distance $S$. For the upper surface, the parameter $S_u$ is defined as the ratio of the chordwise surface distance of a point from the leading edge of the model to the surface length of the model. For the lower surface, the parameter $S_\ell$ is defined as the ratio of the chordwise surface distance of a point from the expansion corner to the true length of the model aft of the expansion corner. With this artifice we have presented the data for both the upper and lower surfaces on the same graph page.

4

For model B we have presented the data at two chordwise stations versus the semispan Y and wedge height Z. The Nusselt number for this model is based on the x projection of a point. There is a degree of arbitrariness in using the projection, especially for the wedge, and we do not attribute any physical significance to this presentation.

The data for model A are presented in Figs. 7 through 22; those for model B in Figs. 23 through 30. The symbols are defined in the figures. Whenever a run was repeated the symbols are flagged, and filled symbols are used whenever the Reynolds number per foot was higher than $10^5$. Schlieren photographs were obtained throughout the program; some are presented in Figs. 31, 32, and 33.

In Ref. 2 we reported on the use of Krylon white enamel as a heat sensitive paint and recommended its use for preliminary, qualitative investigations of complicated configurations, which have many areas of interaction. A winged re-entry configuration was tested in the AEDC Hotshot 2 tunnel and clearly defined regions of ·reased aerodynamic heating were observed. Two runs were      in the present test ser·es using the Krylon white enamel pai.. . Photographs of model A before and after the run and model B after the run are presented in Figs. 34, 35, and 36. Although hot areas can be seen in these pictures, there exists a lack of detail, which can be attributed in part to the considerably shorter duration of the GHST test runs. The use of Krylon is best employed for preliminary analyses of complicated configurations in test facilities having longer test durations.

## REFERENCES

1. Evans, W. J., and Kaufman, L. G. II, <u>Pretest Report on Hypersonic Flow Separation and Control Models for AEDC Tunnels A, B, Hotshot 2 and Grumman Hypersonic Shock Tunnel</u>, Grumman Research Department Memorandum RM-209, July 1962.

2. Hartofilis, S. A., <u>Pressure Measurements at Mach 19 for a Winged Re-entry Configuration</u>, ASD-TDR-63-319, May 1963.

3. Hopkins, H. B., Scheuing, R. A., and Leng, J., <u>Investigation of Pressure Distributions over Planar, Twisted and Cambered Wings in a Hypersonic Shock Tunnel</u>, ASD-TDR-62-171, May 1962.

4. Wallace, A. R., and Swain, W. N., <u>Pressure Distribution Tests on a 60° and 70° Delta Wing at Mach Numbers 20 to 22</u>, AEDC-TN-61-14, February 1961, CONFIDENTIAL REPORT.

5. Kaufman, L. G. II, <u>Pressure and Heat Transfer Measurements for Hypersonic Flows Over Expansion Corners and Ahead of Ramps</u>, ASD-TDR-63-679, Part I: Mach 5 and 8 Data for Expansion Corner Flows, September 1963, Part II: Mach 5 Pressure Data for Flows Ahead of Ramps, September 1963, Part III: Mach 8 Pressure Data for Flows Ahead of Ramps, December 1963, Part IV: Mach 8 Heat Transfer Data for Flows Ahead of Ramps, to be published.

6. Baer, A. L., <u>An Investigation of Separated Flows on Two-Dimensional Models at Mach Numbers 5 and 8</u>, AEDC-TDR-63-200, October 1963.

7. Burchfield, C. G., Hube, F. K., and Burdette, J. E., <u>An Experimental Heat-Transfer Investigation in Regions of Flow Separation at Mach Number 8</u>, AEDC-TDR-64-30, February 1964.

8. Kaufman, L. G. II, <u>Pressure Measurements for Mach 8 Flows Over Expansion Corners and Ramps on an Internally Cooled Model</u>, RTD-TDR-63-4044, Part I: Expansion Corner Flows, October 1963, Part II: Flows Over a Flat Plate with and without a Partial Span Ramp, to be published, Part III: Flows Over Full Span Ramps Mounted on a Flat Plate, to be published.

6

9.  Kaufman, L. G. II, and Meckler, L. H., Pressure and Heat Transfer Measurements at Mach 5 and 8 for a Fin - Flat Plate Model, ASD-TDR-63-235, April 1963.

10. Kaufman, L. G. II, Pressure Distributions and Oil Film Photographs for Mach 5 Flows Past Fins Mounted on a Flat Plate, ASD-TDR-63-755, September 1963.

11. Kaufman, L. G. II, Pressure Measurements for Mach 5 Flows Over Winged Re-entry Configurations with Aerodynamic Controls, RTD-TDR-63-4179, Part I:  Blunt Cabin Configuration, February 1964, Part II:  Conical Cabin Configuration, February 1964.

12. Meckler, L., Pressure Measurements at Mach 8 on an Aero-dynamically Controllable Winged Re-entry Configuration, to be published as an FDL Technical Documentary Report.

13. Meckler, L., Heat Transfer Measurements at Mach 8 on an Aerodynamically Controllable Winged Re-entry Configuration, to be published as an FDL Technical Documentary Report.

14. Donaldson, J. C., Hypersonic Control Effectiveness Tests of a Delta-Winged Re-entry Configuration at Mach 5 and 8, AEDC-TDR-63-268, December 1963.

15. Lacey, J. J., Jr., Pressure Tests on a Blunt Delta Wing Vehicle at M = 19, AEDC-TDR-63-32, February 1963.

16. Meckler, L., Static Aerodynamic Characteristics at Mach 5 and 8 for an Aerodynamic Controllable Winged Re-entry Configuration, FDL-TDR-64-10, to be published.

17. Kaufman, L. G. II, Pressure Measurements for Mach Five Flows Over a Blunt Pyramidal Configuration with Aerodynamic Controls, RTD-TDR-63-4239, January 1964.

18. Kaufman, L. G. II, Pressure and Heat Transfer Measurements for Mach 8 Flows Over a Blunt Pyramidal Configuration with Aerodynamic Controls, FDL-TDR-64-2, Part I:  Pressure Data for Delta Wing Surface, January 1964, Part II:  Pressure Data for Dihedral Surfaces and Part III:  Heat Transfer Data for Delta Wing Surface, to be published, and Part IV:  Heat Transfer Data for Dihedral Surfaces, May 1964.

19. Donaldson, J. C., _Hypersonic Control Effectiveness Tests of a Blunted, Triangular-Pyramid Re-entry Configuration at Mach 5 and 8,_ AEDC-TDR-63-250, December 1963.

20. Evans, W. J., and Kaufman, L. G. II, _Aerodynamic Characteristics and Flap Loads for a Blunt Pyramidal Configuration at Mach 5 and 8,_ to be published as an FDL Technical Documentary Report.

21. Kaufman, L. G. II, _Pressure and Heat Transfer Measurements for Mach 21 Flows Over a Blunt Pyramidal Configuration with Aerodynamic Controls,_ to be published as an FDL Technical Documentary Report.

# TABLE I.

## INSTRUMENTATION COORDINATES FOR MODEL A

| | Pressure Orifices | | | Heat Transfer Gauges | |
|---|---|---|---|---|---|
| Tap | x | y | Gauge | x | y |
| 1 | 2.43 | -.250 | 1 | 2.43 | .500 |
| 2 | 2.93 | -.500 | 2 | 2.93 | .250 |
| 3 | 3.42 | -.250 | 3 | 3.42 | .500 |
| 4 | 2.688 | .250 | 4 | 2.688 | -.500 |
| 5 | 3.188 | .500 | 5 | 3.188 | -.250 |
| 6 | 3.688 | .250 | 6 | 3.688 | -.500 |
| 7 | 4.188 | .500 | 7 | 4.188 | -.250 |
| 8 | 4.750 | .250 | 8 | 4.750 | -.500 |
| 9 | 5.25 | .500 | 9 | 5.25 | -.250 |
| 10 | 5.75 | .250 | 10 | 5.75 | -.500 |

## TABLE II

### INSTRUMENTATION COORDINATES FOR MODEL B

#### Pressure Orifices

| Tap | $x_{in}$ | $y_{in}$ | $z_{in}$ |
|-----|----------|----------|----------|
| 1 | .875 | 0 | 0 |
| 2 | 1.375 | 0 | |
| 3 | 1.875 | 0 | |
| 4 | 3.000 | .462 | |
| 5 | 3.000 | .900 | |
| 6 | 3.000 | 1.650 | |
| 7 | 4.500 | .862 | |
| 8 | 4.500 | 1.300 | 0 |
| 9 | 3.000 | - .400 | -1.500 |
| 10 | 3.250 | .400 | -1.500 |
| 11 | 3.000 | .26 | .312 |
| 12 | 4.500 | .67 | .312 |
| 13 | 3.000 | .26 | .937 |
| 14 | 4.500 | .67 | .937 |
| 15 | 4.500 | .67 | 1.437 |

#### Heat Transfer Gauges

| Gauge | $x_{in}$ | $y_{in}$ | $z_{in}$ |
|-------|----------|----------|----------|
| 1 | 1.875 | .900 | 0 |
| 2 | 1.875 | - .900 | |
| 3 | 3.000 | - .462 | |
| 4 | 3.000 | - .900 | |
| 5 | 3.000 | -1.650 | |
| 6 | 4.500 | - .867 | |
| 7 | | -1.300 | 0 |
| 8 | | - .67 | .312 |
| 9 | | - .67 | .937 |
| 10 | 4.500 | - .67 | 1.437 |

TABLE III

## PROGRAM SUMMARY AND TEST CONDITIONS FOR MODEL A

| Run No. | $\alpha$ deg | $\varepsilon$ deg | M | Re/ft x $10^{-5}$ | $T_{o_R}$ | $T_\infty$ R | $P_\infty$ x $10^4$ | $\rho_\infty$ x $10^7$ |
|---|---|---|---|---|---|---|---|---|
| 1254 | 0 | 30 | 13.73 | 1.19 | 3650 | 105.43 | 18.16 | 14.47 |
| 1255 | 0 | | 13.73 | 1.18 | 3495 | 100.25 | 16.72 | 14.01 |
| 1256 | 0 | | 13.73 | 1.18 | 3479 | 99.72 | 16.62 | 14.00 |
| 1409 | -15 | 30 | 13.83 | 1.19 | 3170 | 88.42 | 13.94 | 13.24 |
| 1413 | | 0 | 13.83 | 1.21 | 3022 | 83.81 | 13.03 | 13.06 |
| 1394 | | 0 | 20.50 | 1.45 | 3697 | 48.69 | 4.68 | 8.07 |
| 1395 | | 15 | | 1.19 | 4660 | 64.84 | 5.90 | 7.64 |
| 1397 | -15 | 30 | | 1.39 | 3957 | 52.79 | 5.07 | 8.07 |
| 1400 | -15 | 45 | 20.50 | 1.32 | 4232 | 57.32 | 5.44 | 7.98 |
| 1265 | -10 | 30 | 19.24 | 0.88 | 3517 | 52.08 | 3.33 | 5.37 |
| 1266 | -10 | 30 | | 0.86 | 3657 | 54.50 | 3.50 | 5.40 |
| 1267 | -10 | 45 | | 0.84 | 3791 | 56.84 | 3.66 | 5.41 |
| 1263 | - 5 | 30 | | 0.87 | 3607 | 53.63 | 3.44 | 5.39 |
| 1264 | | 30 | | 0.88 | 3529 | 52.27 | 3.35 | 5.38 |
| 1281 | | 0 | | 0.84 | 3839 | 57.70 | 3.71 | 5.41 |
| 1282 | - 5 | 0 | | 0.84 | 3792 | 56.86 | 3.66 | 5.41 |
| 1257 | 0 | 30 | | 0.87 | 3592 | 53.36 | 3.42 | 5.39 |
| 1269 | | 45 | | 0.84 | 3842 | 57.76 | 3.72 | 5.41 |
| 1270 | | 45 | | 0.85 | 3763 | 56.36 | 3.63 | |
| 1271 | | 15 | | 0.84 | 3849 | 57.88 | 3.73 | |
| 1272 | | 15 | | 0.84 | 3806 | 57.11 | 3.68 | |
| 1275 | | 0 | | 0.85 | 3762 | 56.34 | 3.63 | 5.41 |
| 1276 | | | | 0.86 | 3676 | 54.83 | 3.53 | 5.40 |
| 1380 | | | 19.24 | 1.44 | 3721 | 49.06 | 4.72 | 8.08 |
| 1382 | | 0 | 20.50 | 1.22 | 3918 | 52.16 | 4.37 | 7.03 |
| 1384 | | 15 | | 1.17 | 4047 | 54.25 | 4.44 | 6.87 |
| 1385 | | 30 | | 1.17 | 4109 | 55.27 | 4.58 | 6.97 |
| 1389 | 0 | 45 | 20.50 | 1.43 | 3785 | 50.06 | 4.82 | 8.08 |
| 1260 | 10 | 30 | 19.24 | 0.86 | 3646 | 54.31 | 3.49 | 5.40 |
| 1277 | | 0 | 19.24 | 0.85 | 3772 | 56.51 | 3.64 | 5.41 |
| 1406 | | 45 | 20.50 | 0.80 | 3582 | 50.41 | 2.83 | 4.71 |
| 1408 | 10 | 15 | 20.50 | 0.81 | 3473 | 48.65 | 2.72 | 4.69 |
| 1417 | 30 | 0 | 19.77 | 0.79 | 3723 | 52.74 | 2.97 | 4.73 |
| 1418 | 30 | 15 | 19.77 | 0.82 | 3357 | 46.78 | 2.60 | 4.66 |

## PROGRAM SUMMARY AND TEST CONDITIONS FOR MODEL B

| Run No. | $\alpha$ deg | Wedge | M | Re/ft x $10^{-5}$ | $T_{o_R}$ | $T_\infty$ R | $P_\infty$ x $10^4$ | $\rho_\infty$ x $10^7$ |
|---|---|---|---|---|---|---|---|---|
| 1451 | 0 | Small | 13.83 | 2.35 | 3334 | 93.64 | 29.97 | 26.85 |
| 1450 | | Small | 19.77 | 0.82 | 3373 | 47.05 | 2.61 | 4.67 |
| 1447 | | Large | 13.88 | 2.33 | 3412 | 96.15 | 30.91 | 27.01 |
| 1448 | | | 13.88 | 2.22 | 3780 | 108.30 | 35.22 | 27.31 |
| 1446 | | | 19.77 | 0.83 | 3321 | 46.22 | 2.56 | 4.65 |
| 1449 | 0 | Large | 19.77 | 0.81 | 3463 | 48.49 | 2.71 | 4.69 |
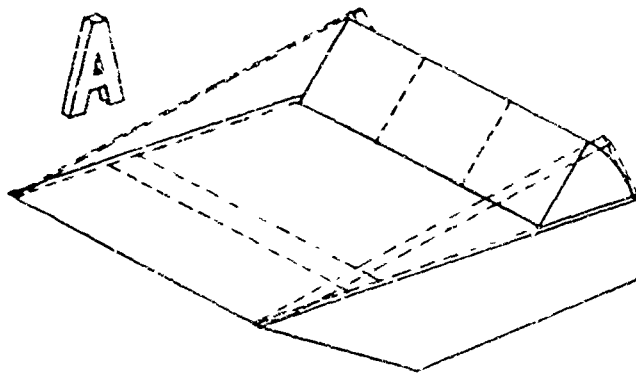
Separated Flows ahead of a Ramp
Fore and aft flaps, end plates
3 separate models:

1) Pressure and heat transfer, AEDC Tunnels
A & B, M = 5 & 8, results in Refs. 5-7.

2) Controlled wall temperature, pressure,
AEDC Turnel B, M = 8, results in Refs. 6 and 8.

3) Pressure and heat transfer, Grumman Shock
Tunnel, $M \approx 13$ & 19, results herein.
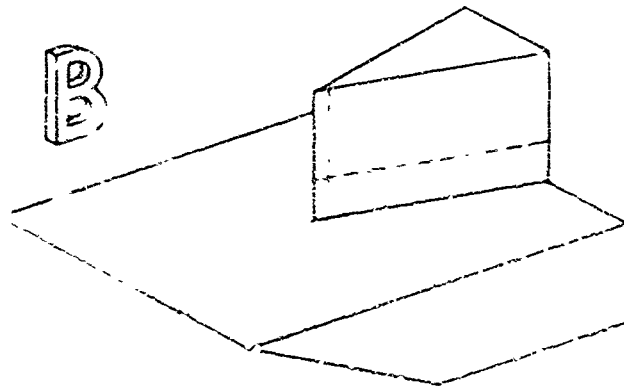
Wedge - Plate Interaction
Small and large fins with sharp
and blunt leading edges
2 separate models:

1) Pressure and heat transfer, AEDC Tunnels
A & B, M = 5 & 8, results in Refs. 6,7,9 and 10.

2) Pressure and heat transfer, Grumman Shock
Tunnel, $M \approx 13$ & 19, results herein.
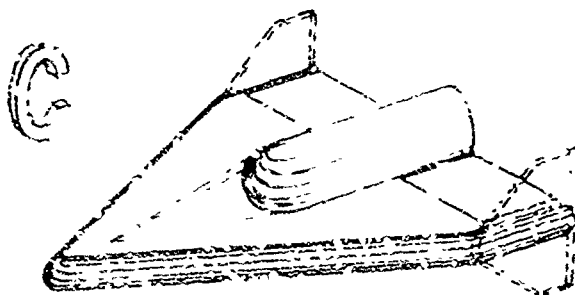
Clipped Delta, Blunt L.E.
Center body, T.E. flaps, drooped nose,
spoiler. tip fins
3 separate models:

1) Pressure and heat transfer, AEDC Tunnels
A & B, M = 5 & 8, results in Refs. 7 and 11-14.

2) Pressure, AEDC Hotshop 2,
$M \approx 19$, results in Refs. 2 and 15.

3) Six component force, AEDC Tunnels
A & B M = 5 & 8, results in Refs. 14 and 16.
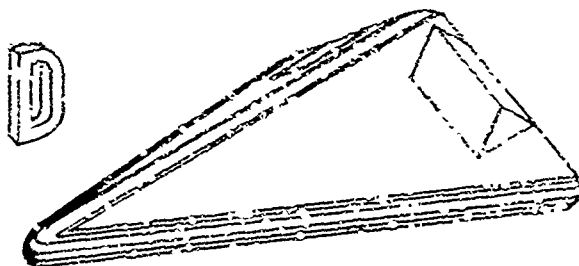
Delta, Blunt L.E., Dihedral
T.E. flaps, canard, ventral fin
3 separate models

1) Pressure and heat transfer, AEDC Tunnels
A & B, M = 5 & 8, results in Refs. 7 and 17-19.

2) Pressure and heat transfer, Grumman Shock
Tunnel, $M \approx 19$, results in Ref. 21.

3) Six component force, AEDC Tunnels
A & B, M = 5 & 8, results in Refs. 19 and 20.

Fig. 1  General Outline of Models and Remarks for Over-all Program

12
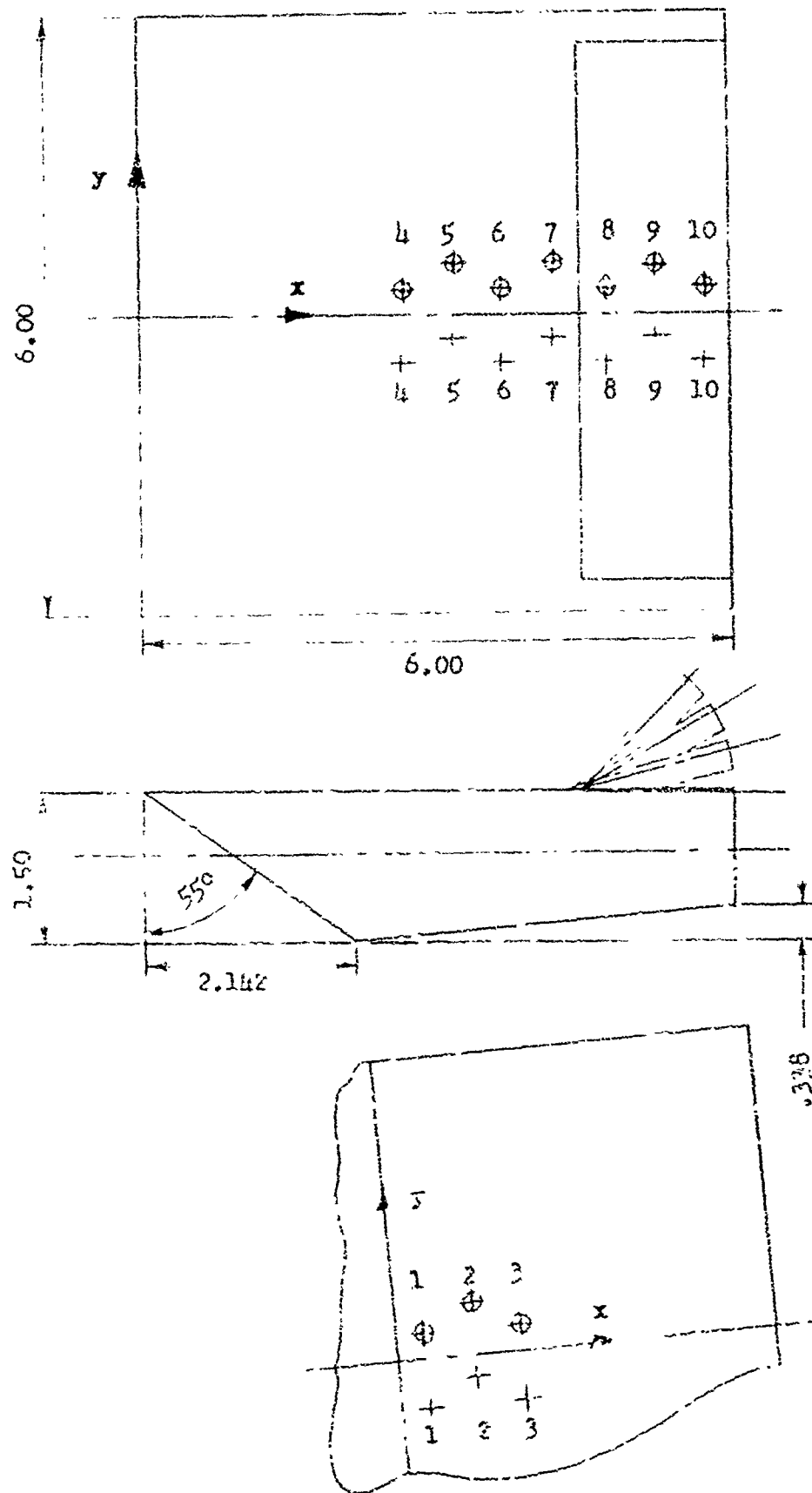
Fig. 2  Dimension and Instrumentation Location for Model A
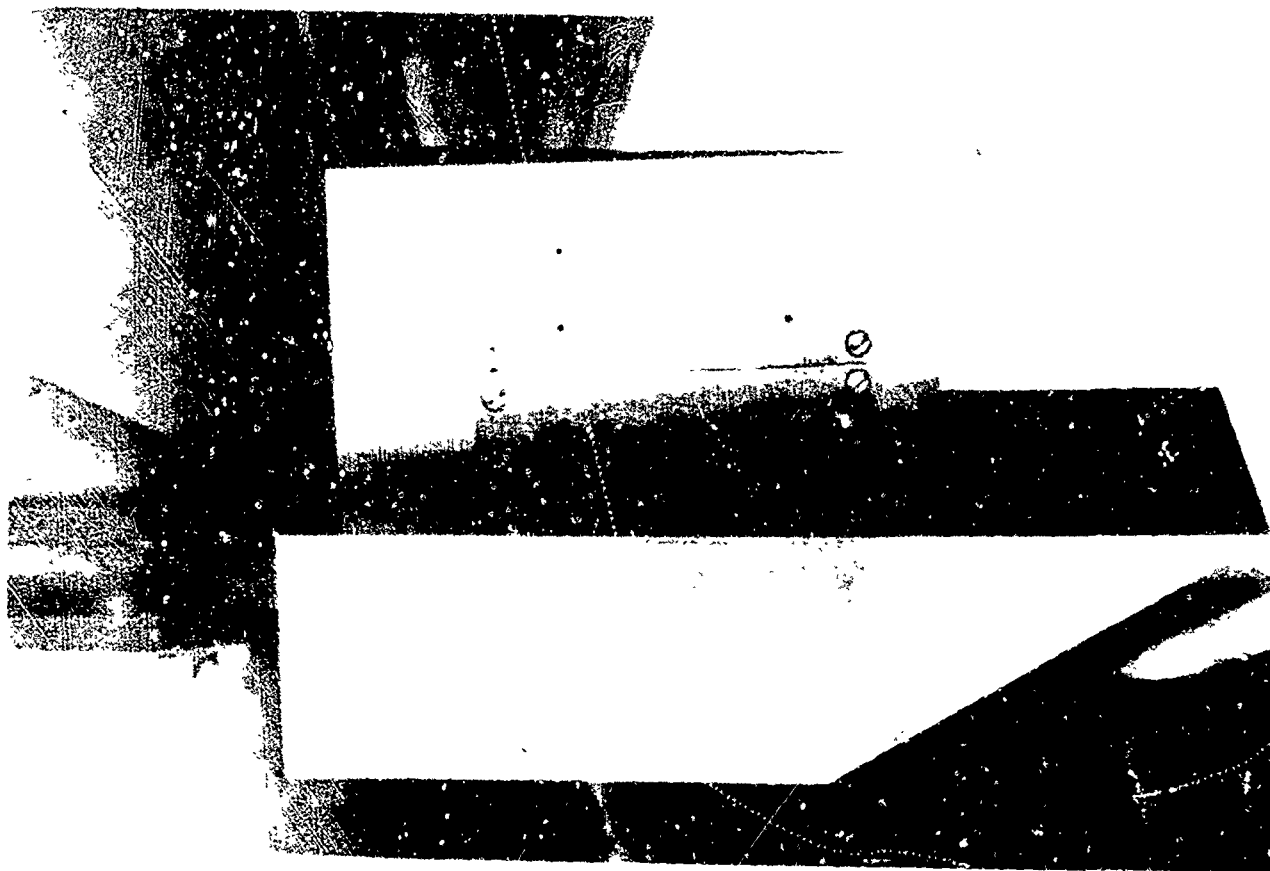
Fig. 3  Photograph Showing Model B with the 2 in. Wedge-Fin
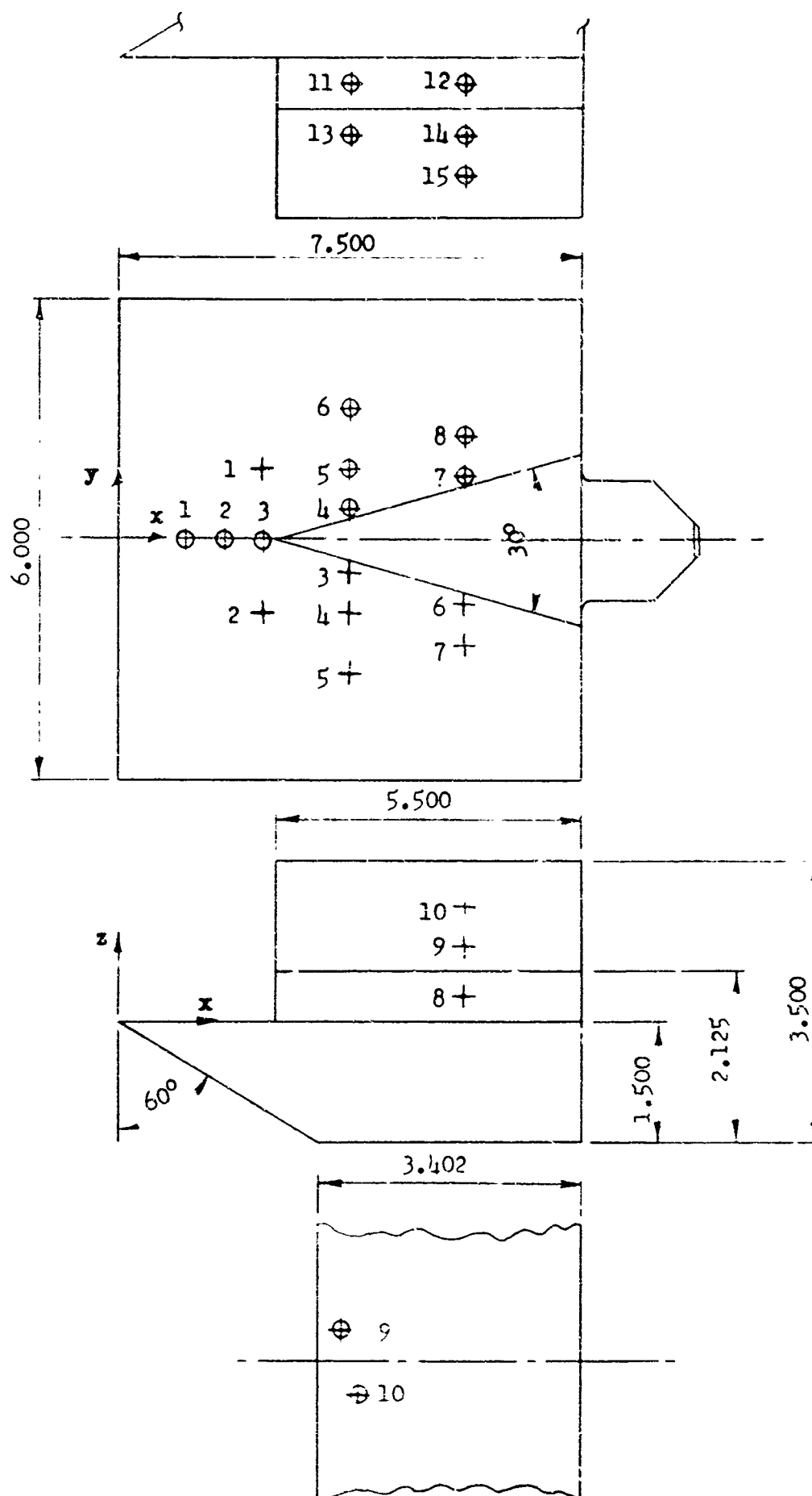
Fig. 4   Dimensions and Instrumentation for Model B
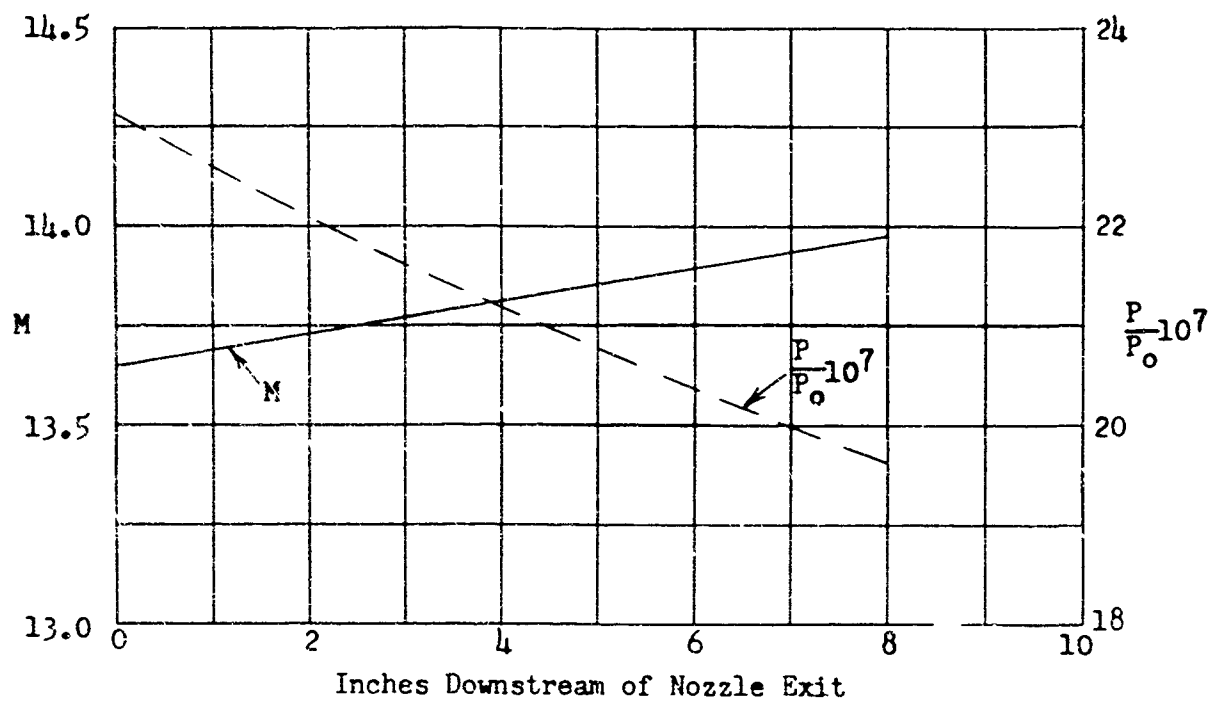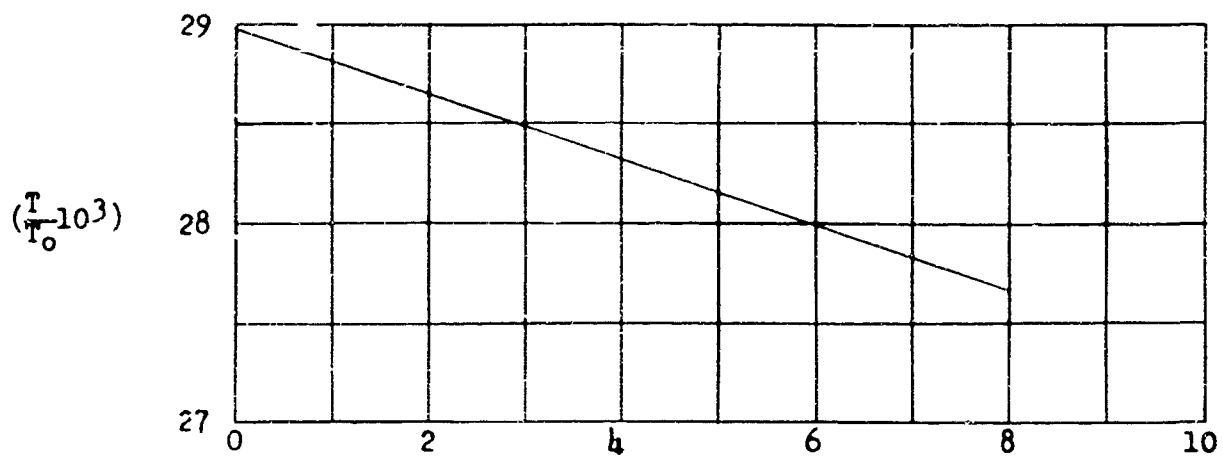
Fig. 5   Tunnel Centerline Distributions of Mach Number and Static
to Total Pressure and Temperature Ratios for the M=13 Conditions

16
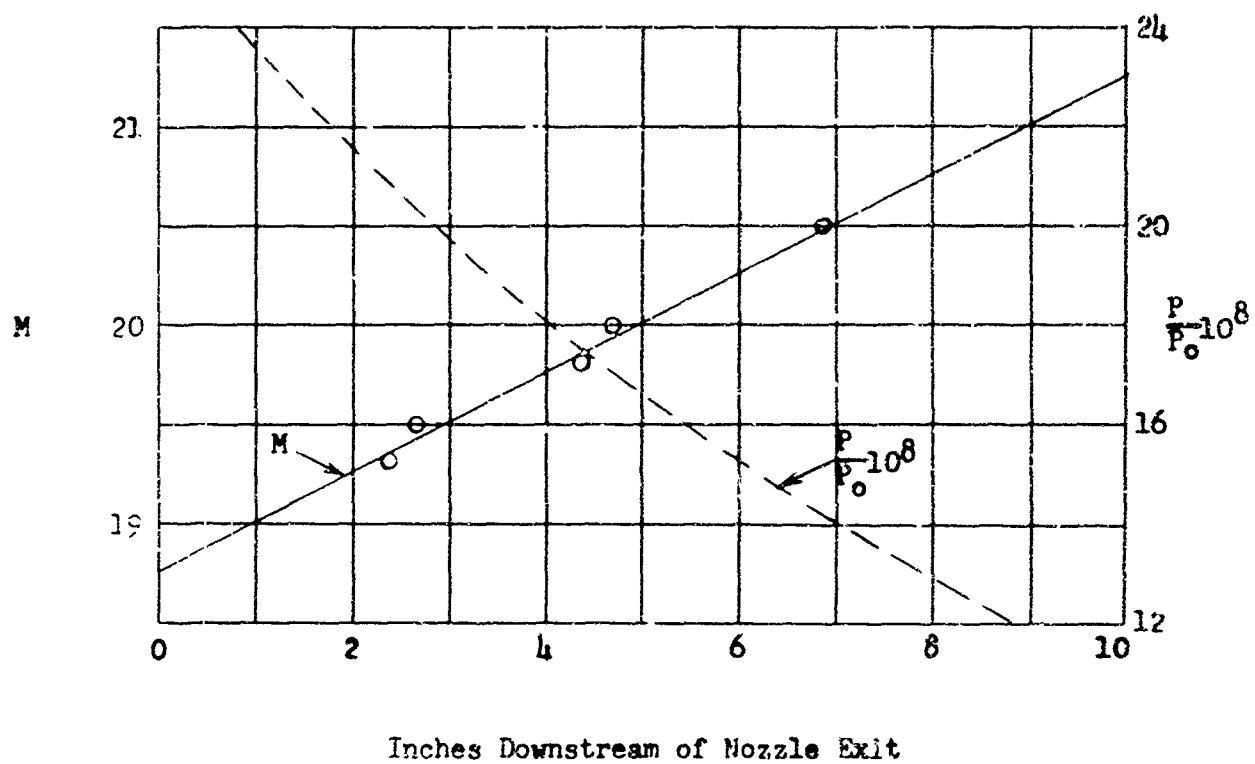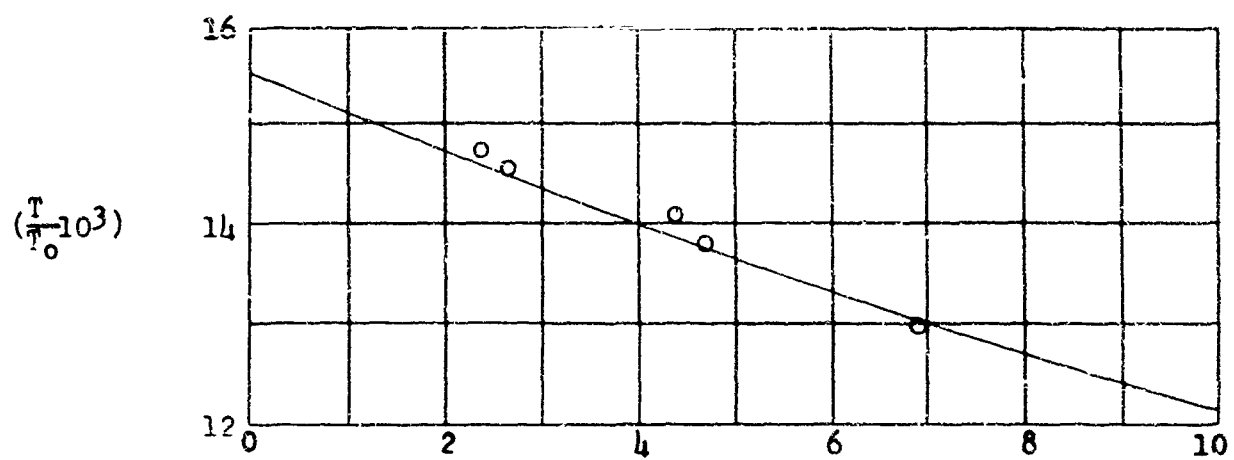
Fig. 6  Tunnel Centerline Distributions of Mach Number and Static to
Total Pressure and Temperature Ratios for the M=19 Conditions

17
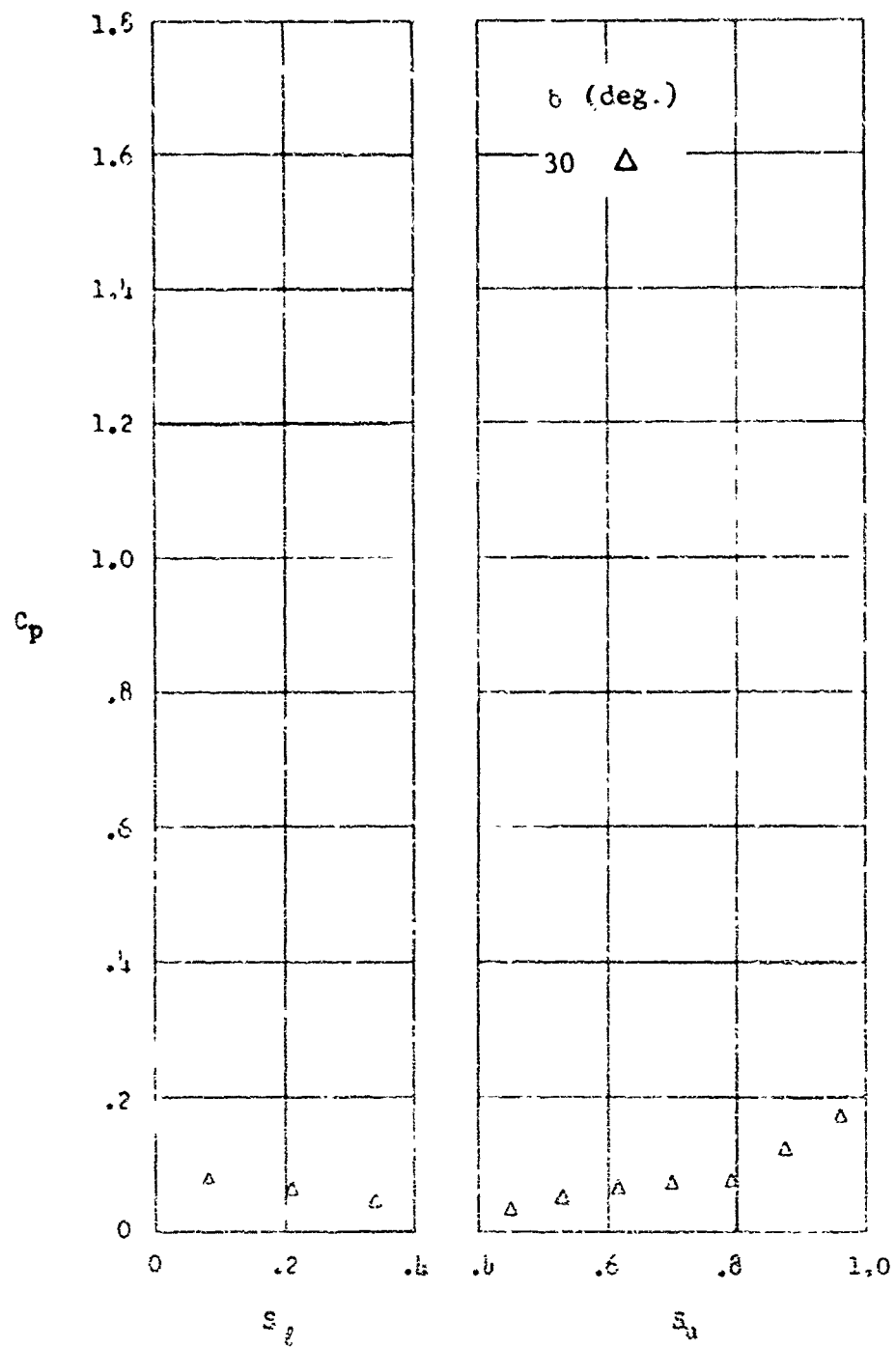
Fig. 7  Chordwise Pressure Distribution for Model A,  $M_\infty \approx 13$, $\alpha \approx 0$

18
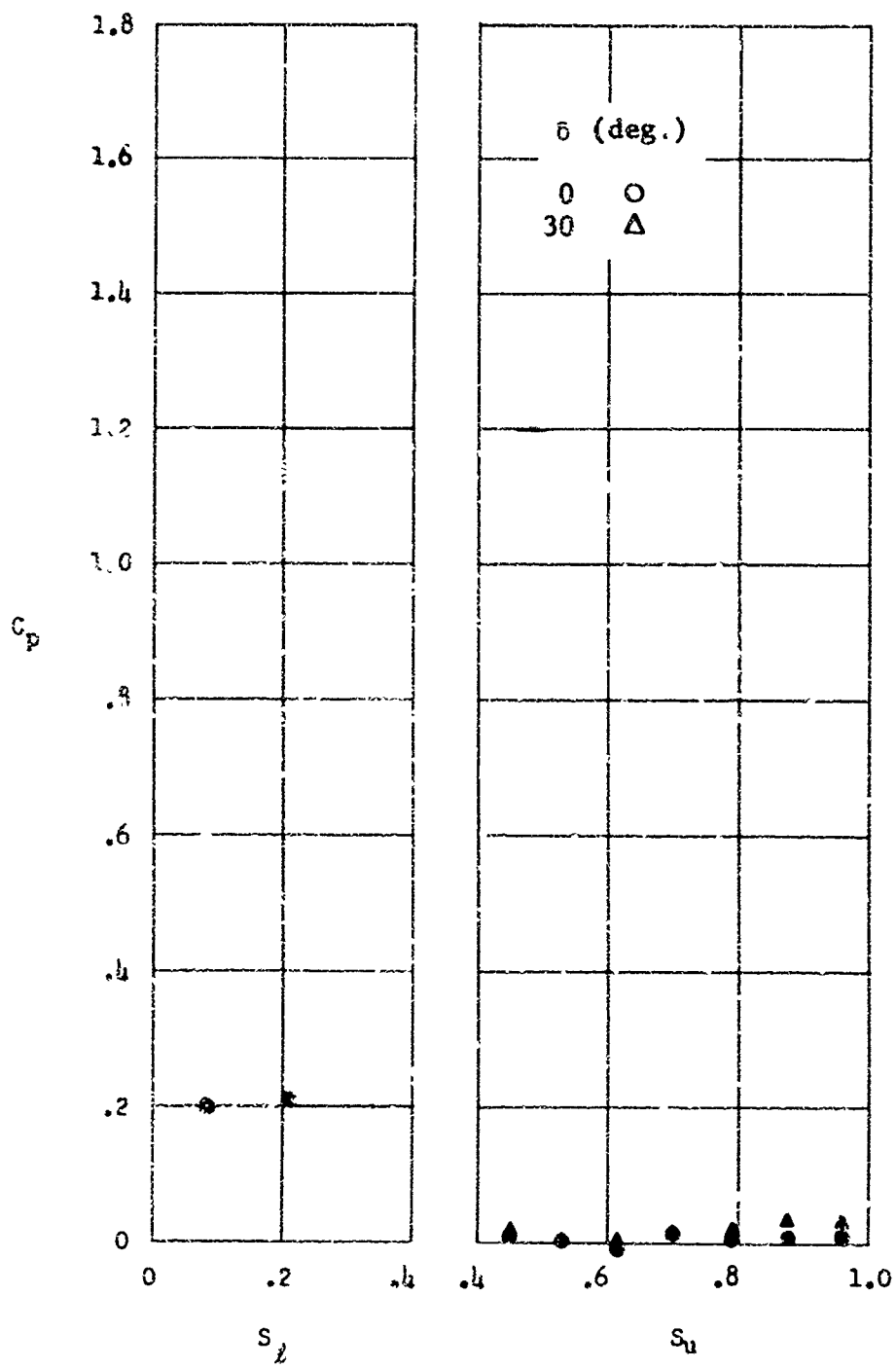
Fig. 8 Chordwise Pressure Distribution for Model A, $M_\infty$ = 13, $\alpha$ = -15
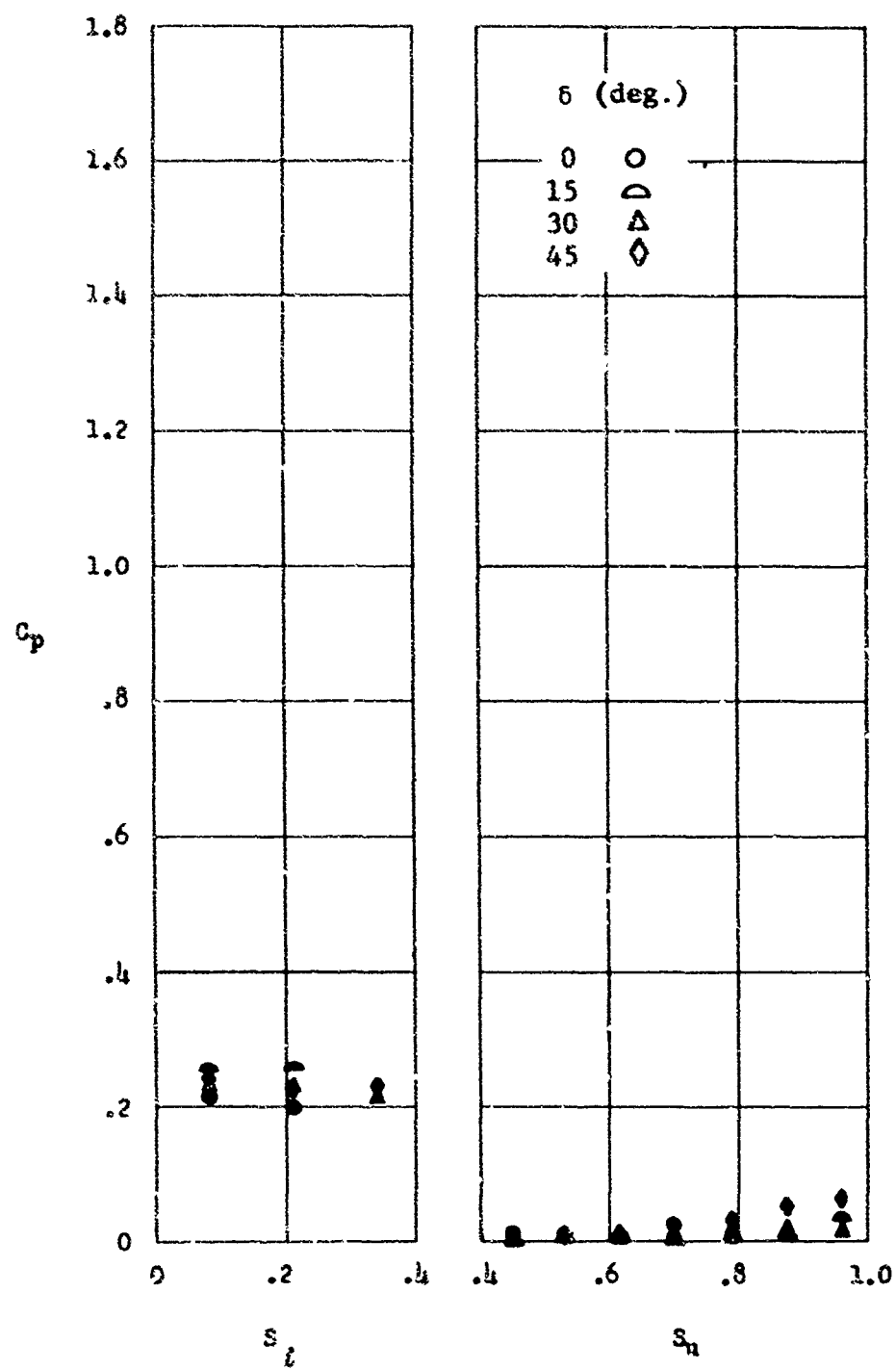
Fig. 9   Chordwise Pressure Distribution for Model A,   $M_\infty = 19$, $\alpha \approx -15$

20
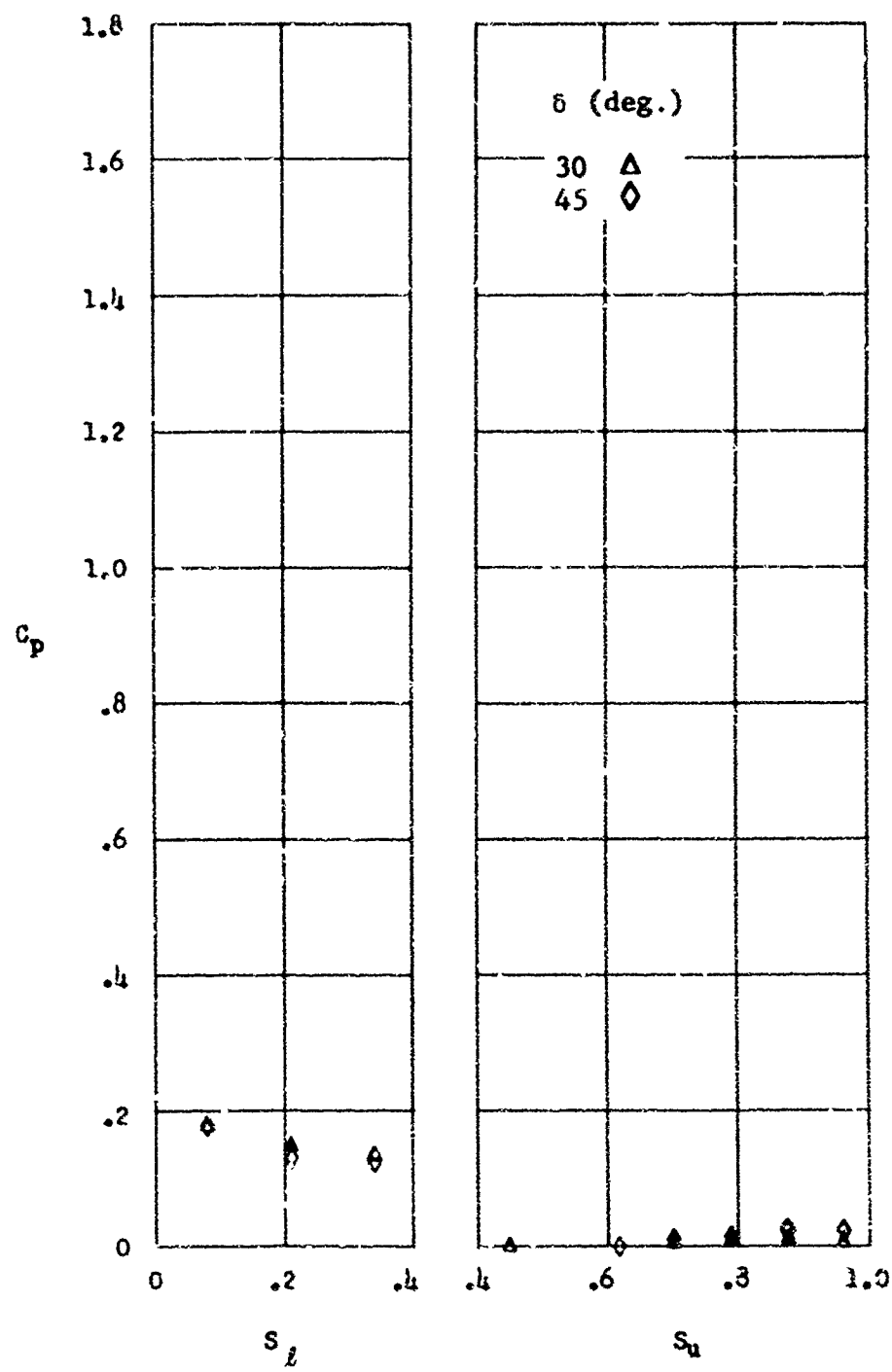
Fig. 10 Chordwise Pressure Distribution for Model A, $M_\infty = 19$, $\alpha = -10$
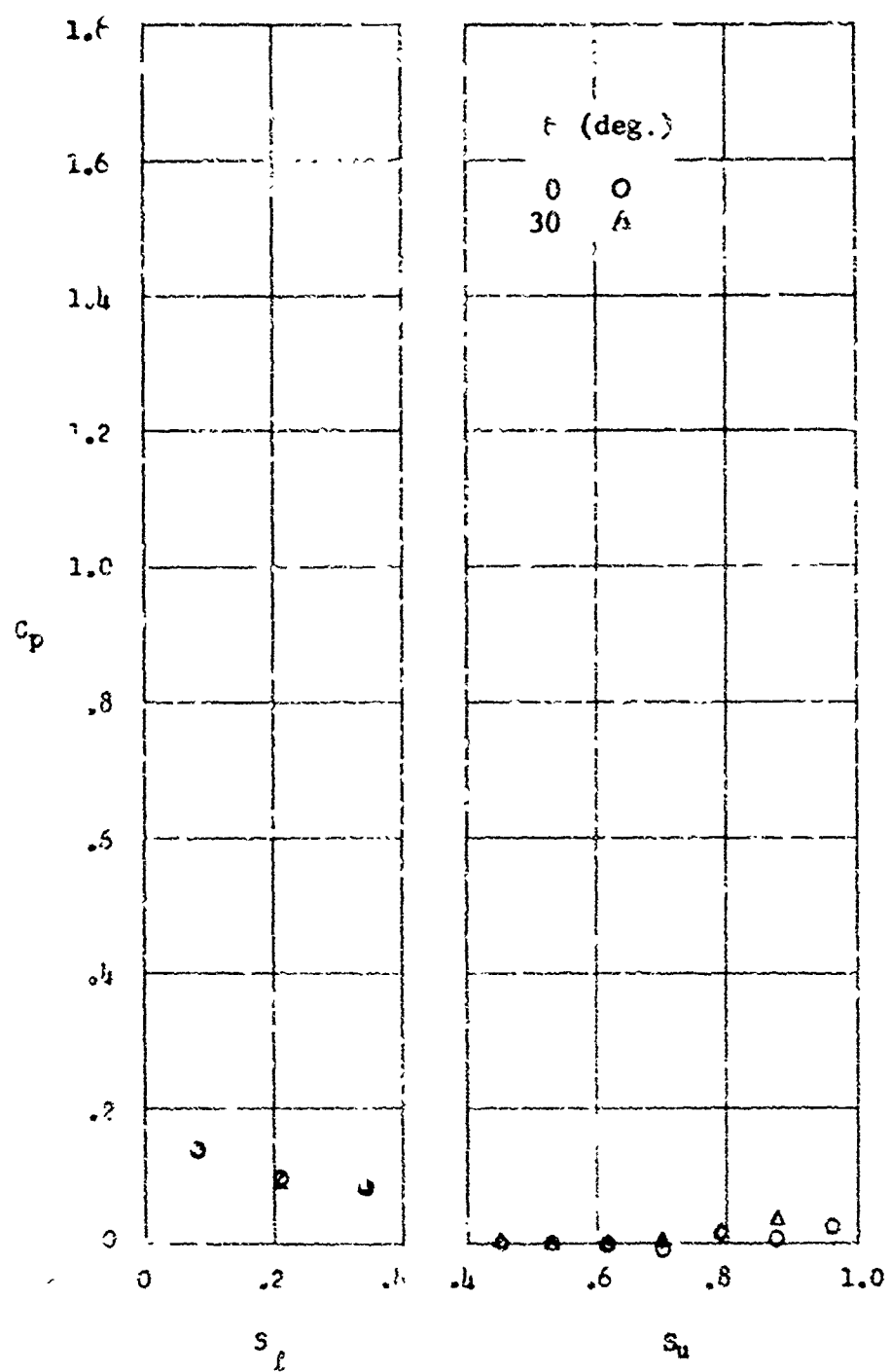
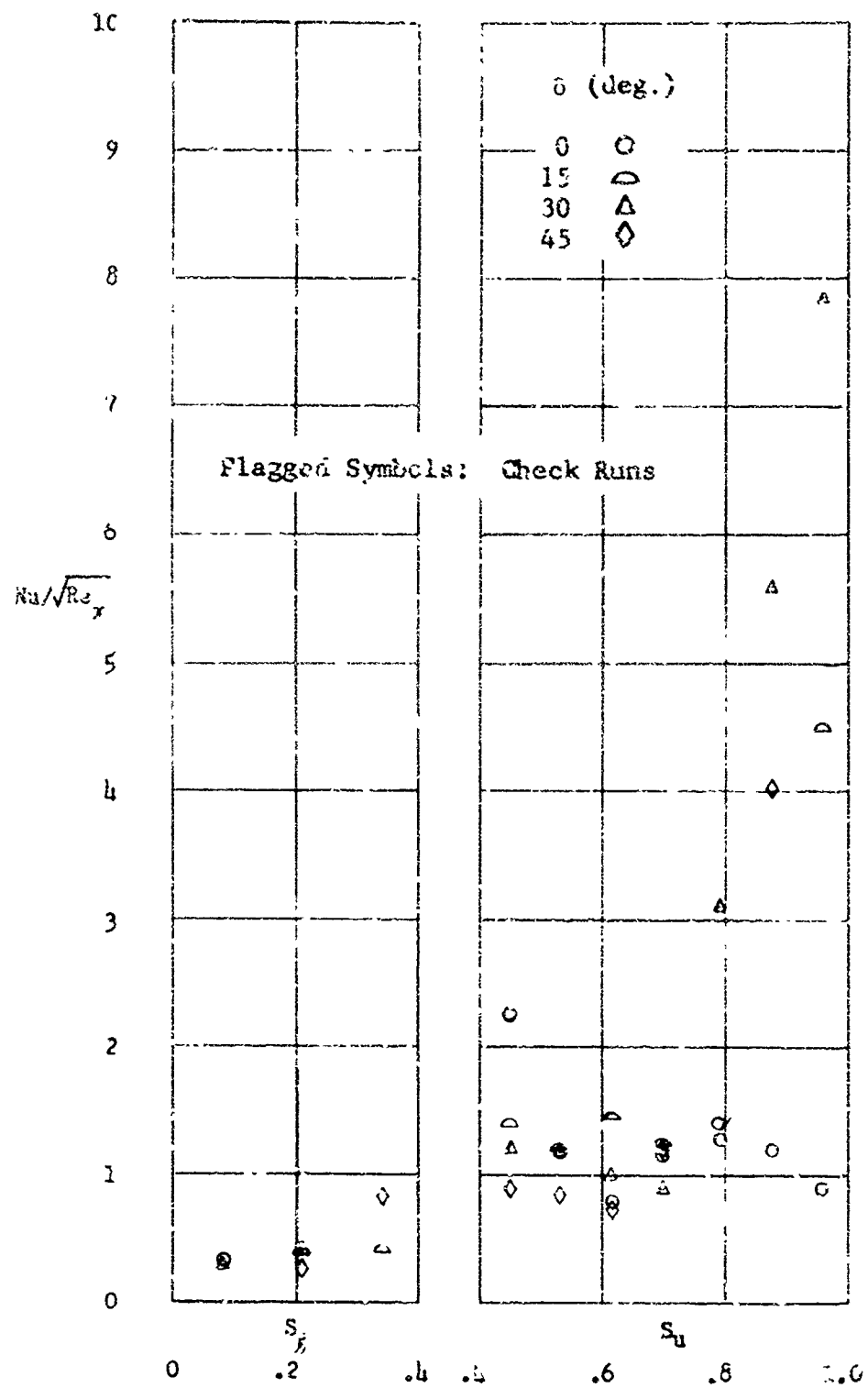Fig. 11  Chordwise Pressure Distribution for Model A, $M_\infty = 19$, $\alpha = -5$
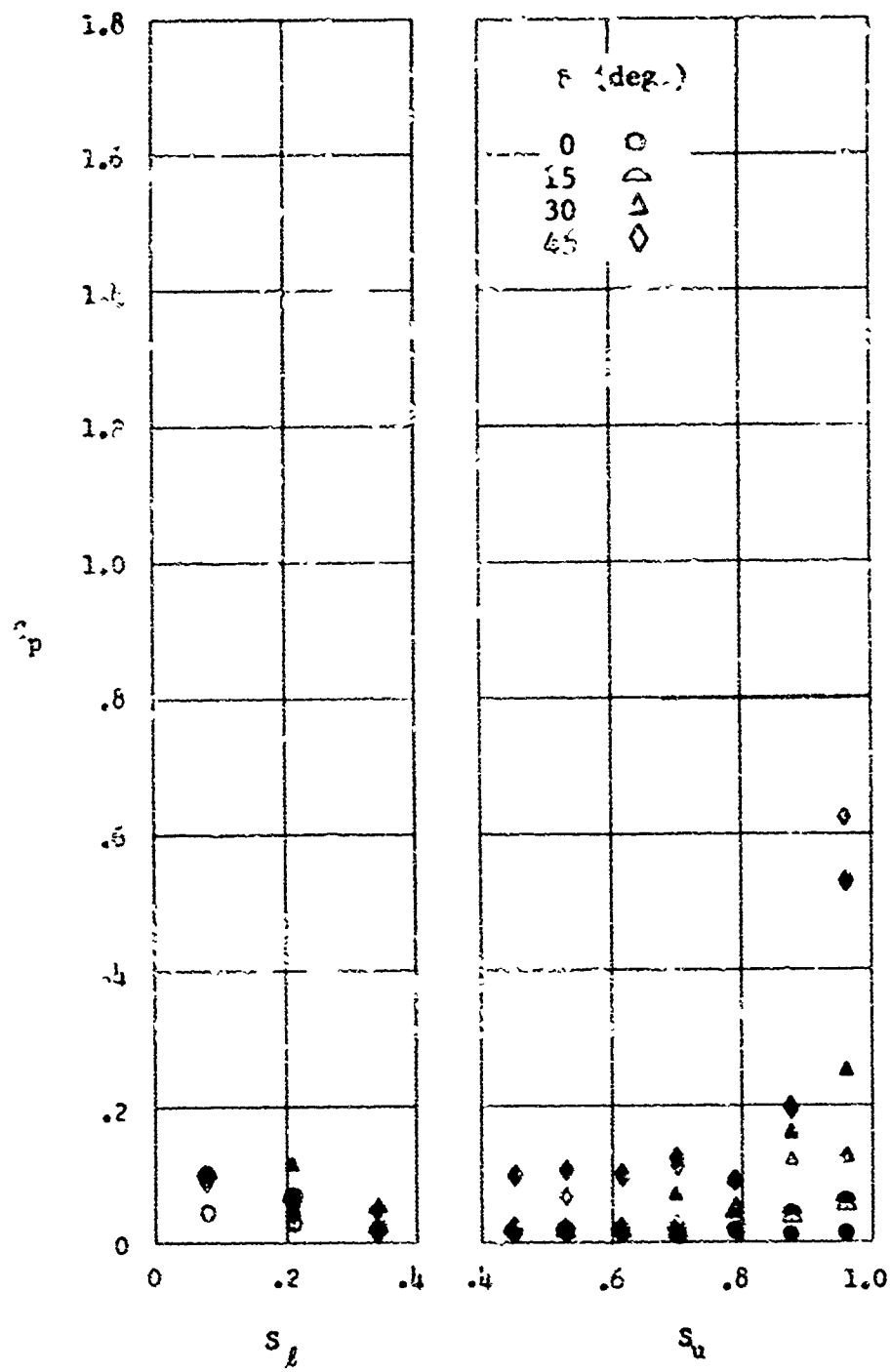
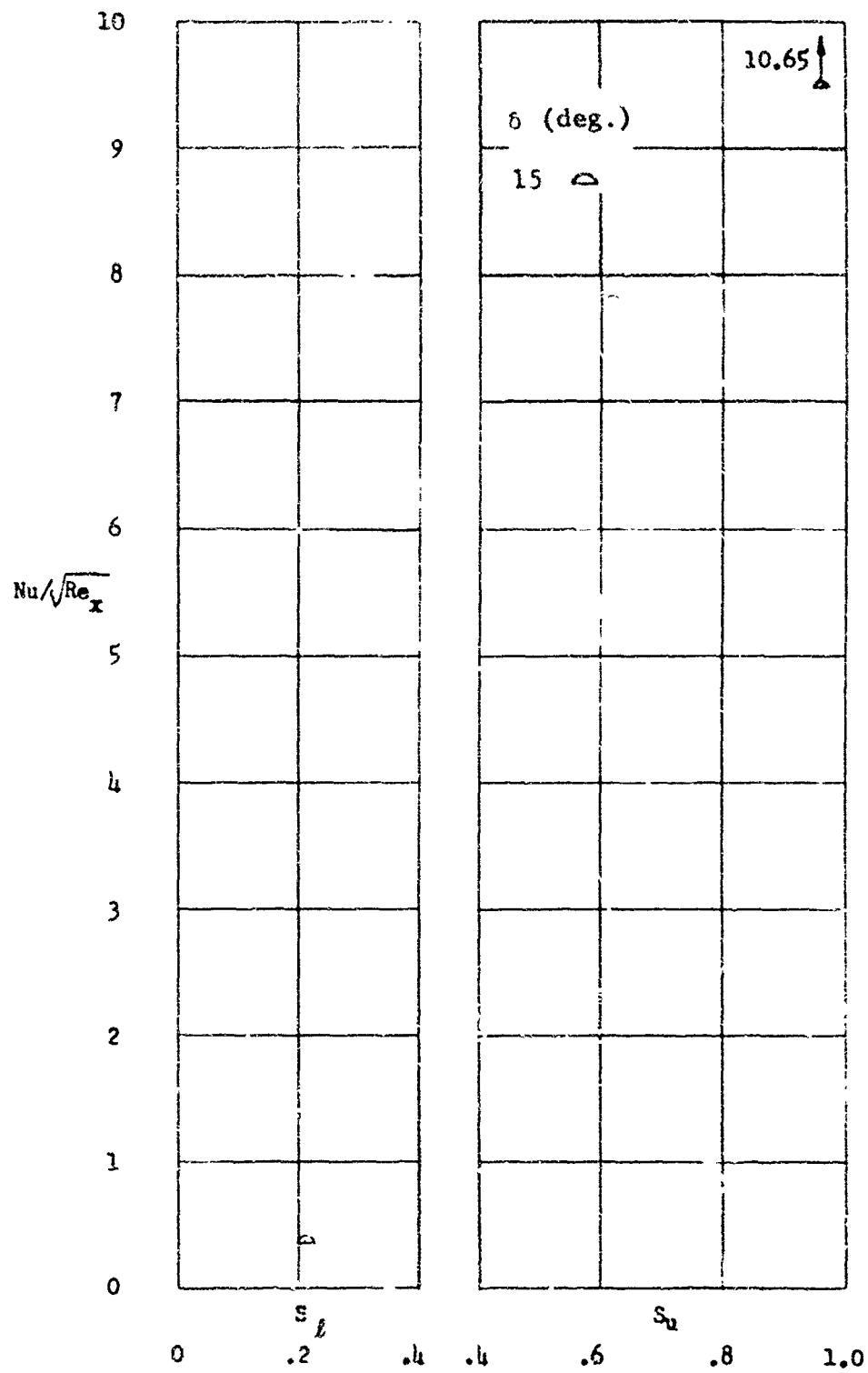Fig. 12 Chordwise Pressure Distribution for Model A, $M_\infty = 19$, $\alpha = 0$

23
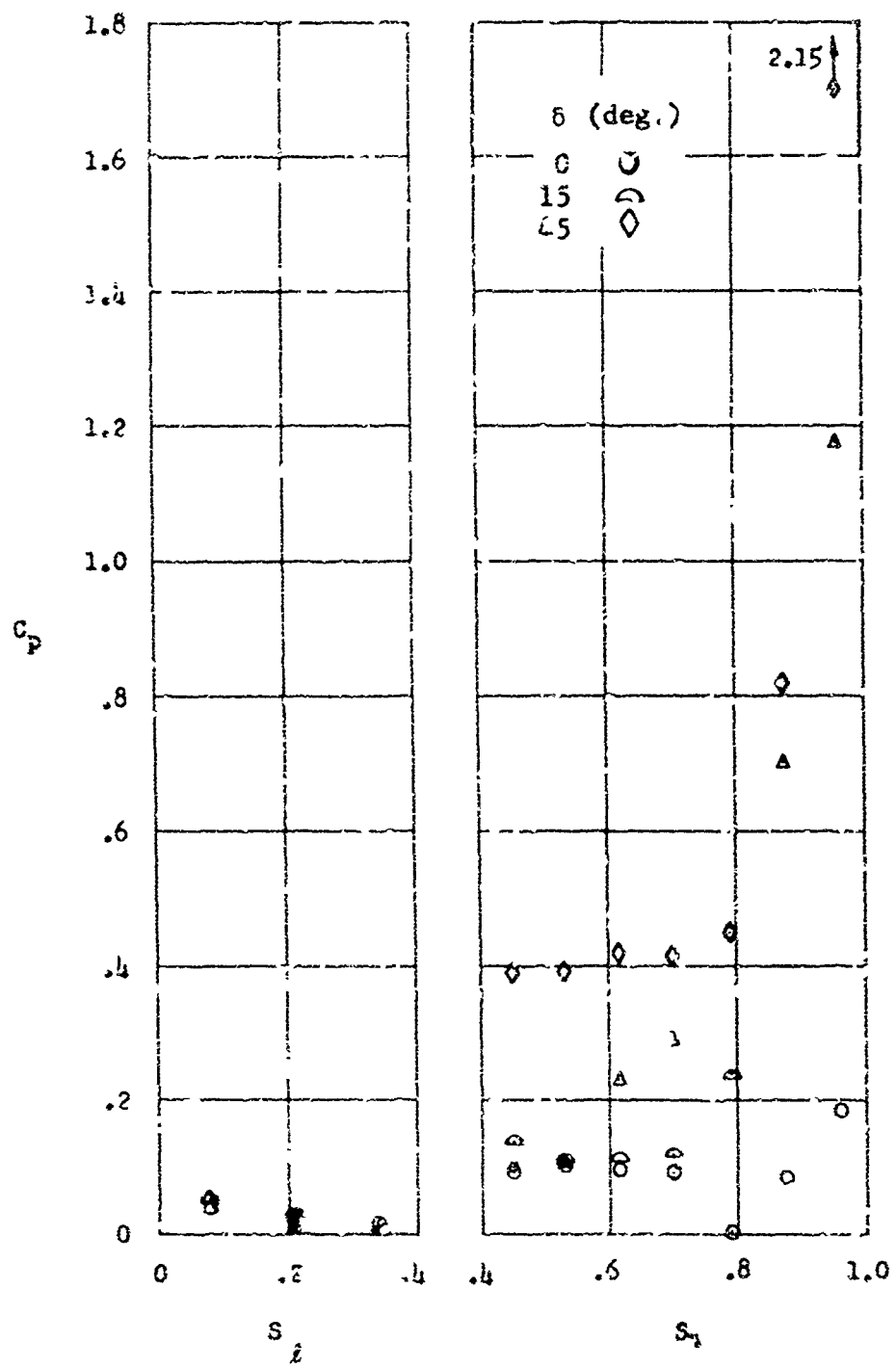
Fig. 13  Chordwise Pressure Distribution for Model A,  $M_\infty = 19$, $\sigma = 10$
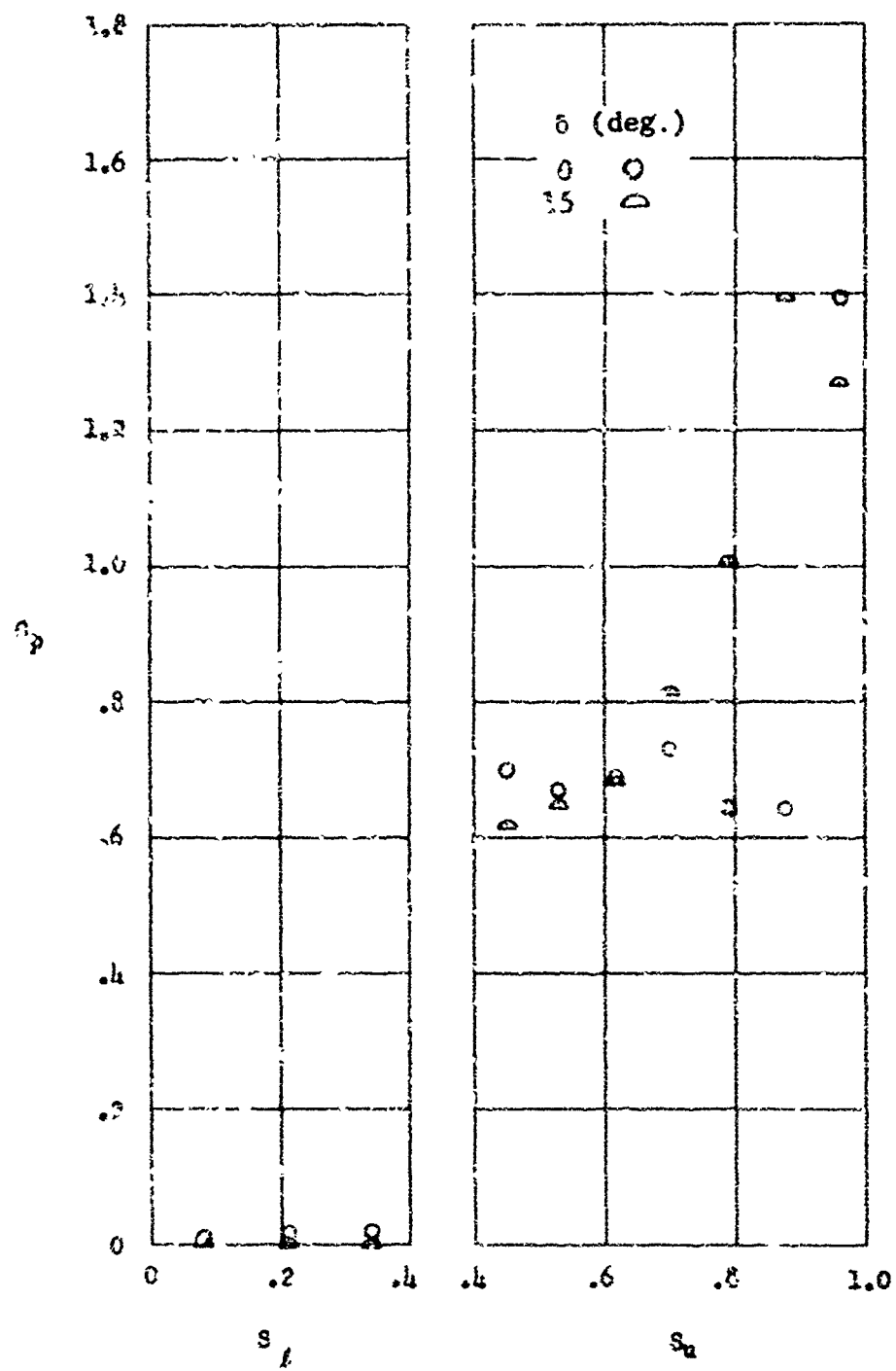
Fig. 14 Chordwise Pressure Distribution for Model A, $M_\infty$ = 19, $\alpha$ = 30

25
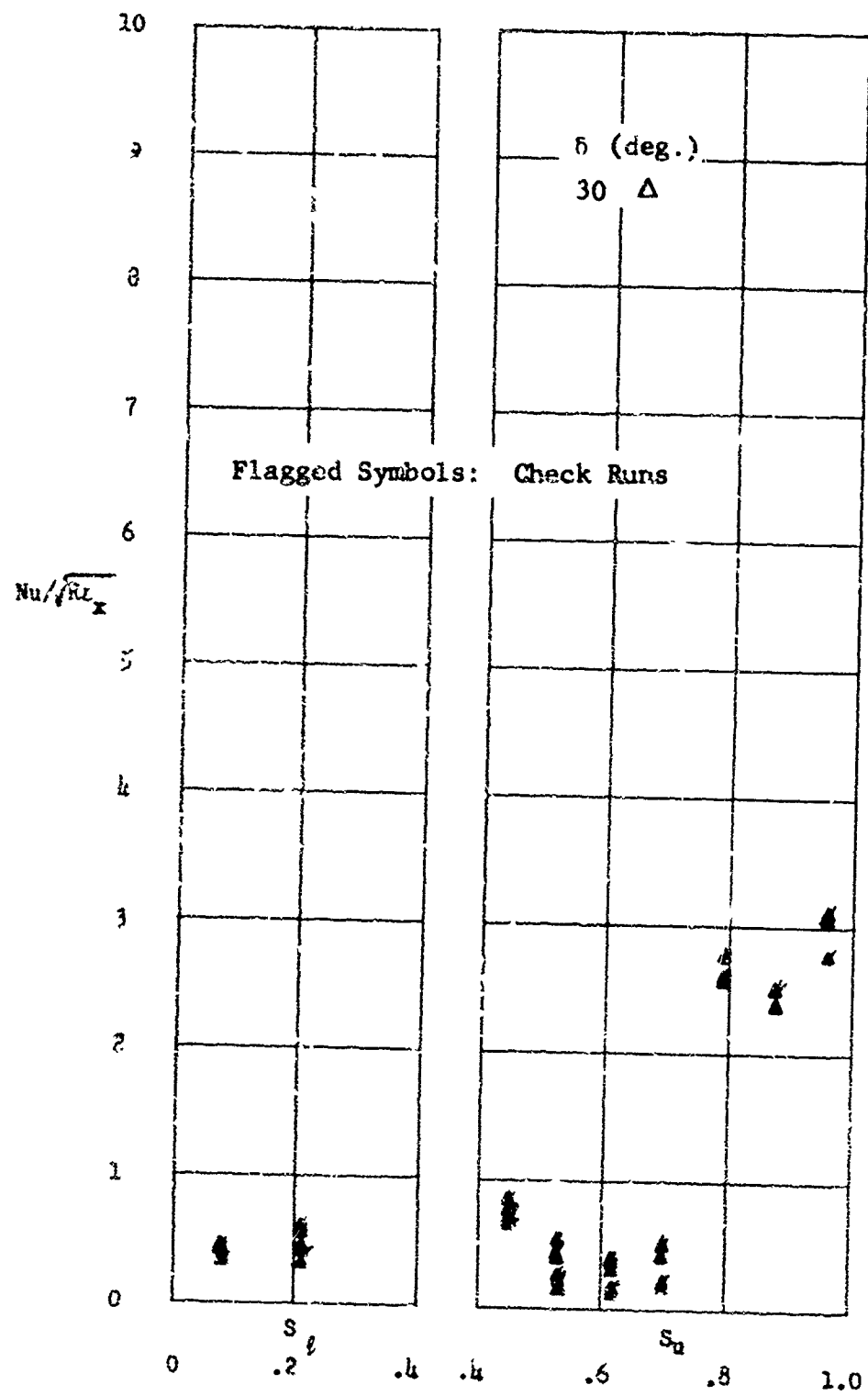
Fig. 15 Chordwise Heat Transfer Distribution for Model A, $M_\infty = 13$, $\alpha = 0$

26

Fig. 16   Chordwise Heat Transfer Distribution for Model A,   $M_\infty$ = 13,  $\alpha$ = -15

27
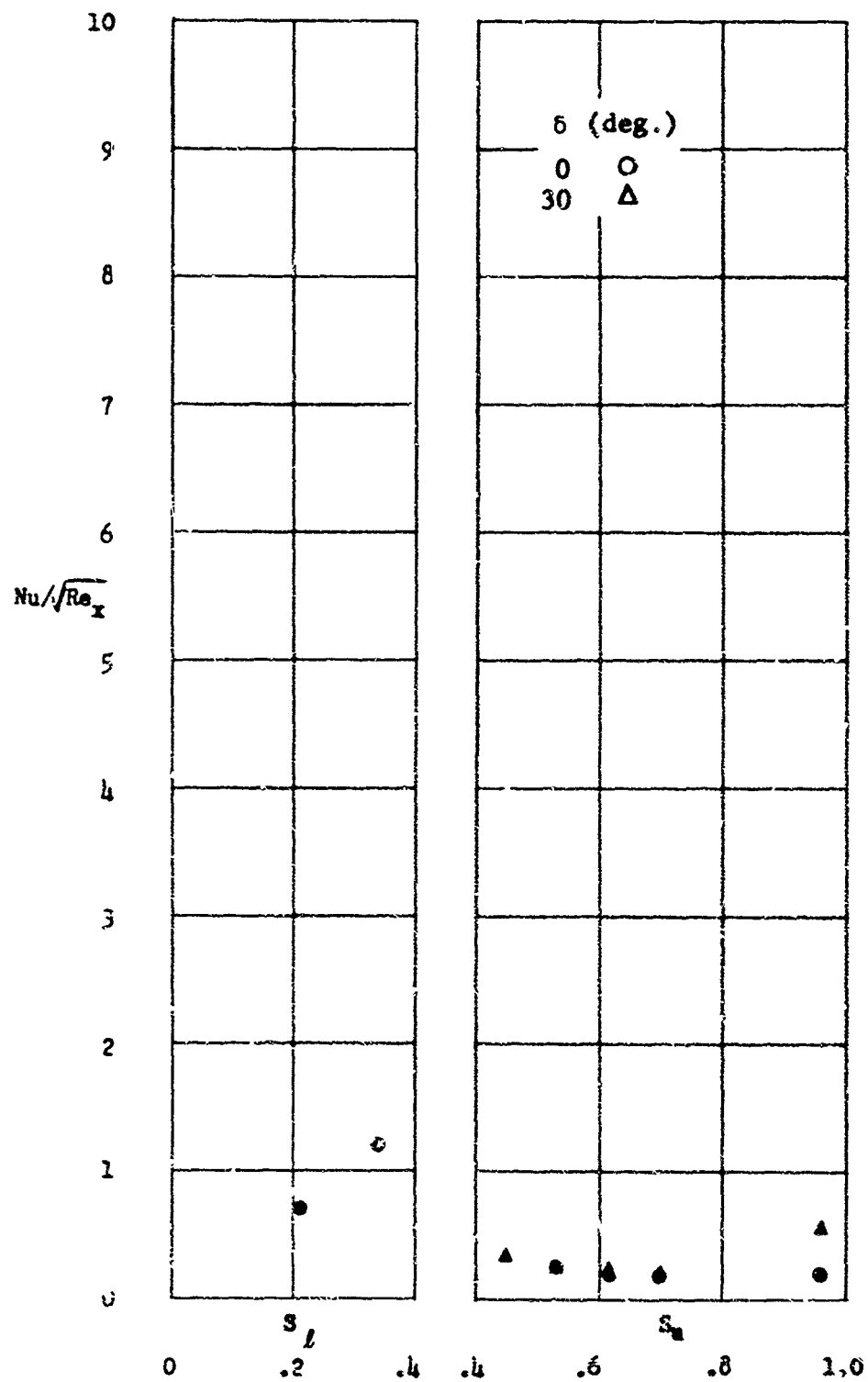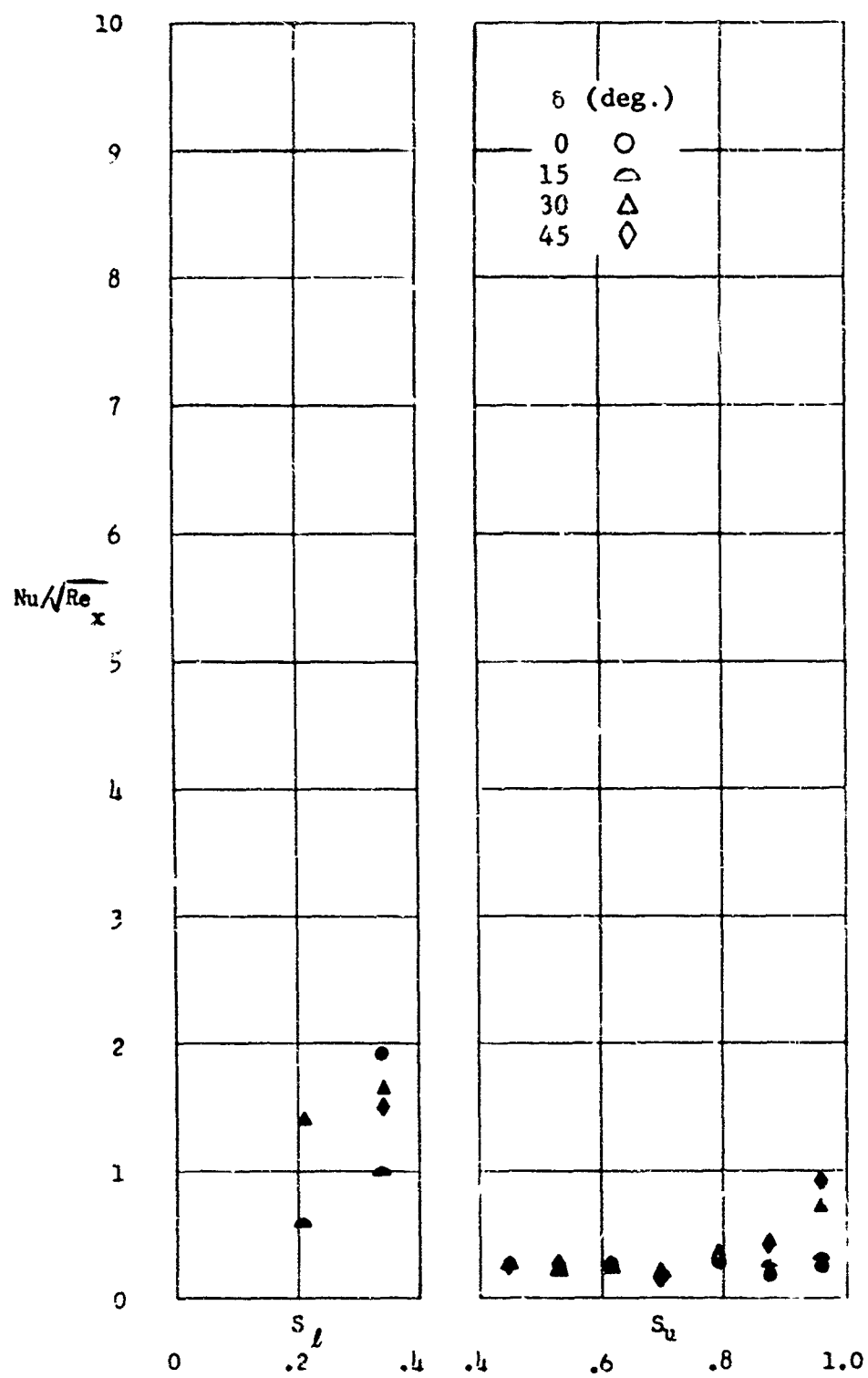
Fig. 17  Chordwise Heat Transfer Distribution for Model A,  $M_\infty = 19$, $\alpha = -15$
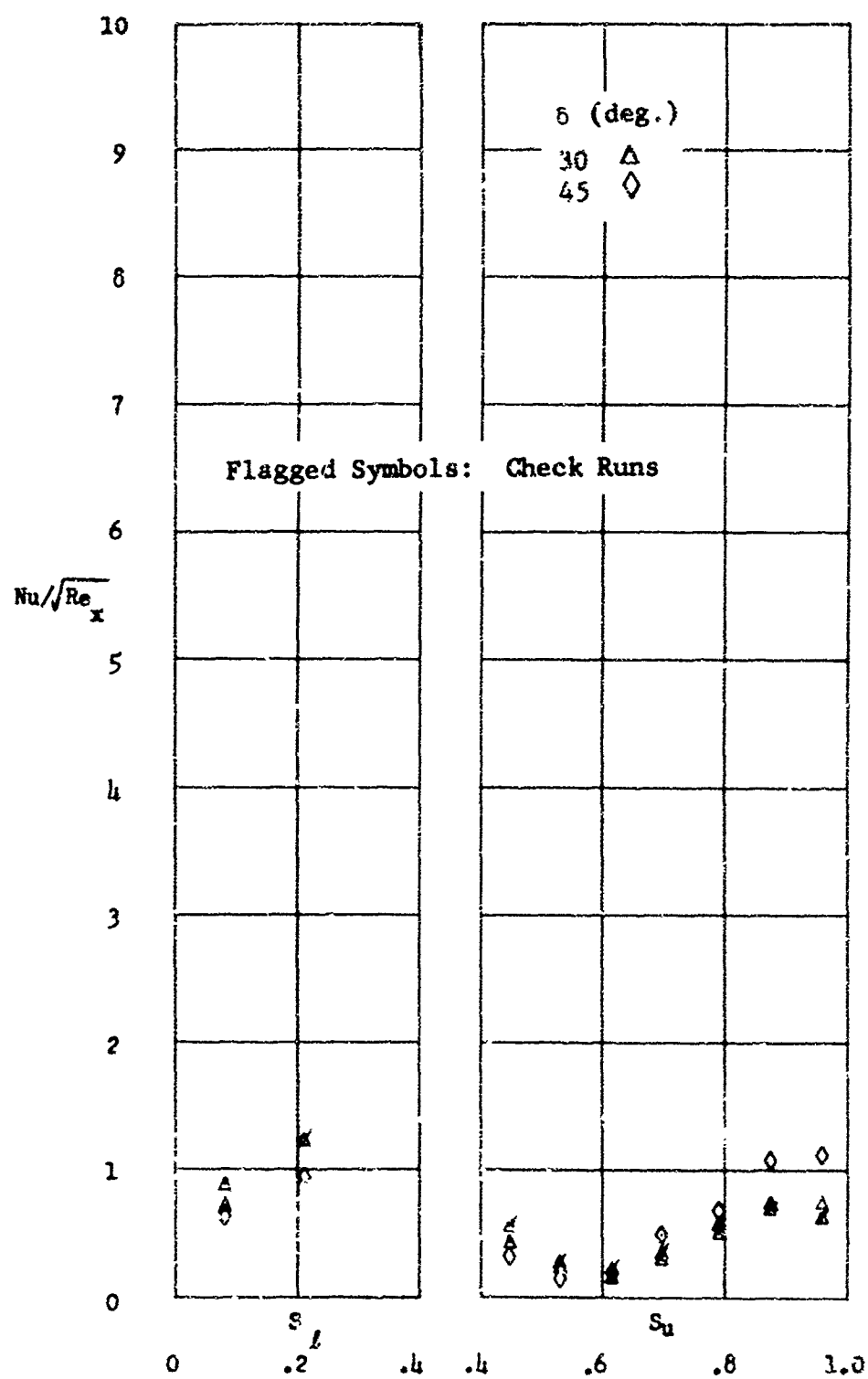
Fig. 16 Chordwise Heat Transfer Distribution for Model A, $M_\infty = 19$, $\alpha = -10$
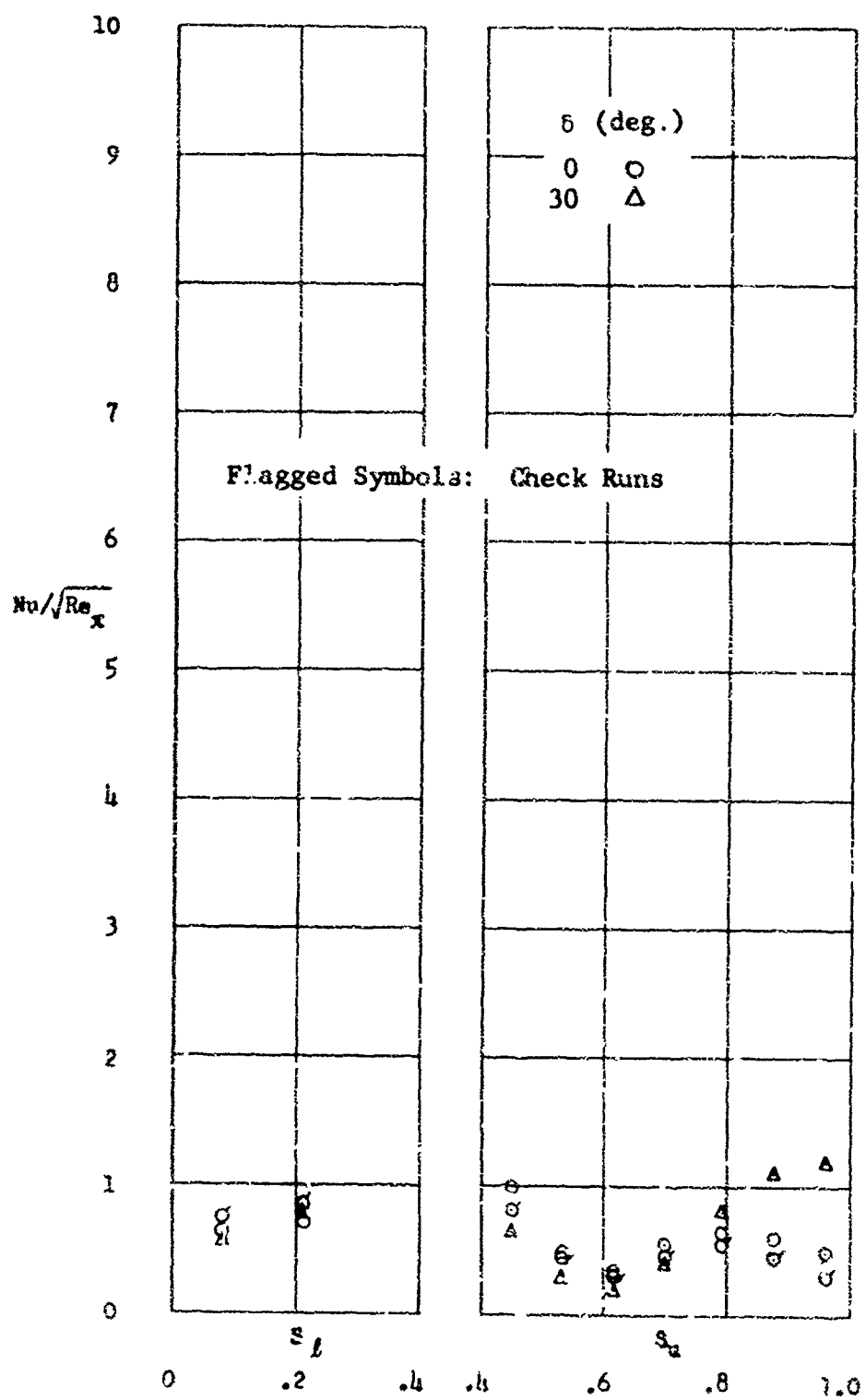
Fig. 19  Chordwise Heat Transfer Distribution for Model A,  $M_\infty = 19$, $\alpha = -5$
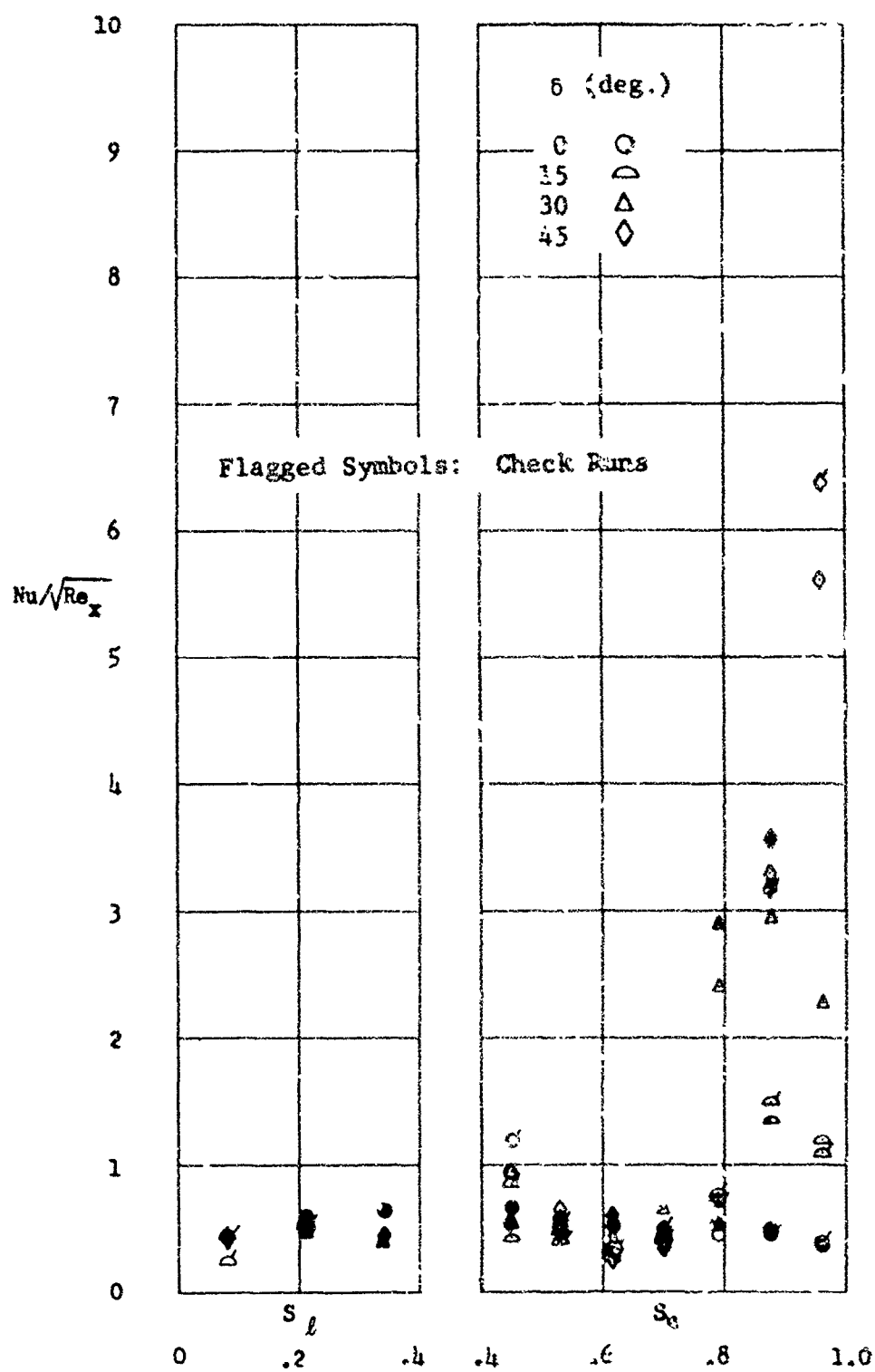
Fig. 20   Chordwise Heat Transfer Distribution for Model A,   $M_\infty = 19$, $\alpha = 0$

Fig. 21 Chordwise Heat Transfer Distribution for Model $A_9$ $M_\infty = 19$, $\alpha = 10$

Fig. 22 Chordwise Heat Transfer Distribution for Model A, $M_\infty = 19$, $\alpha = 30$

33
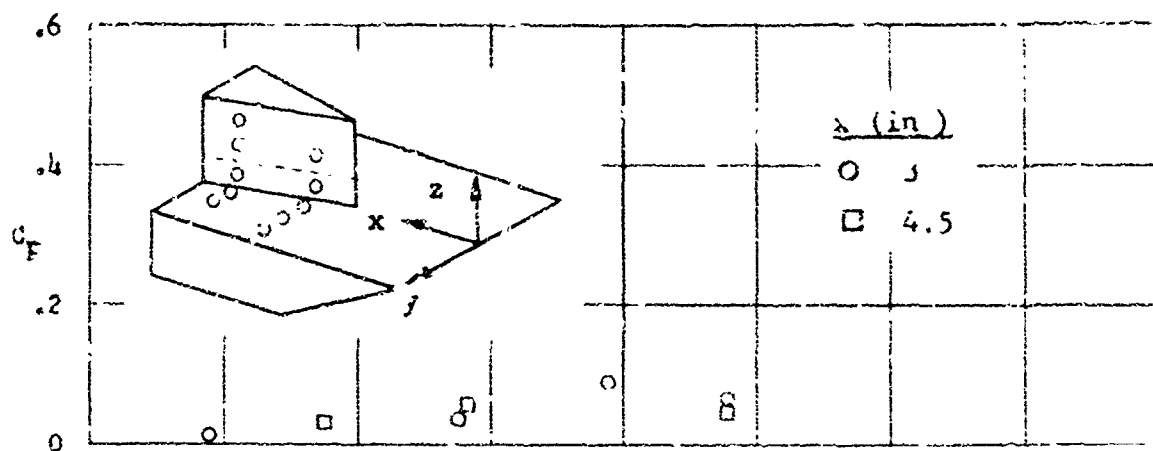
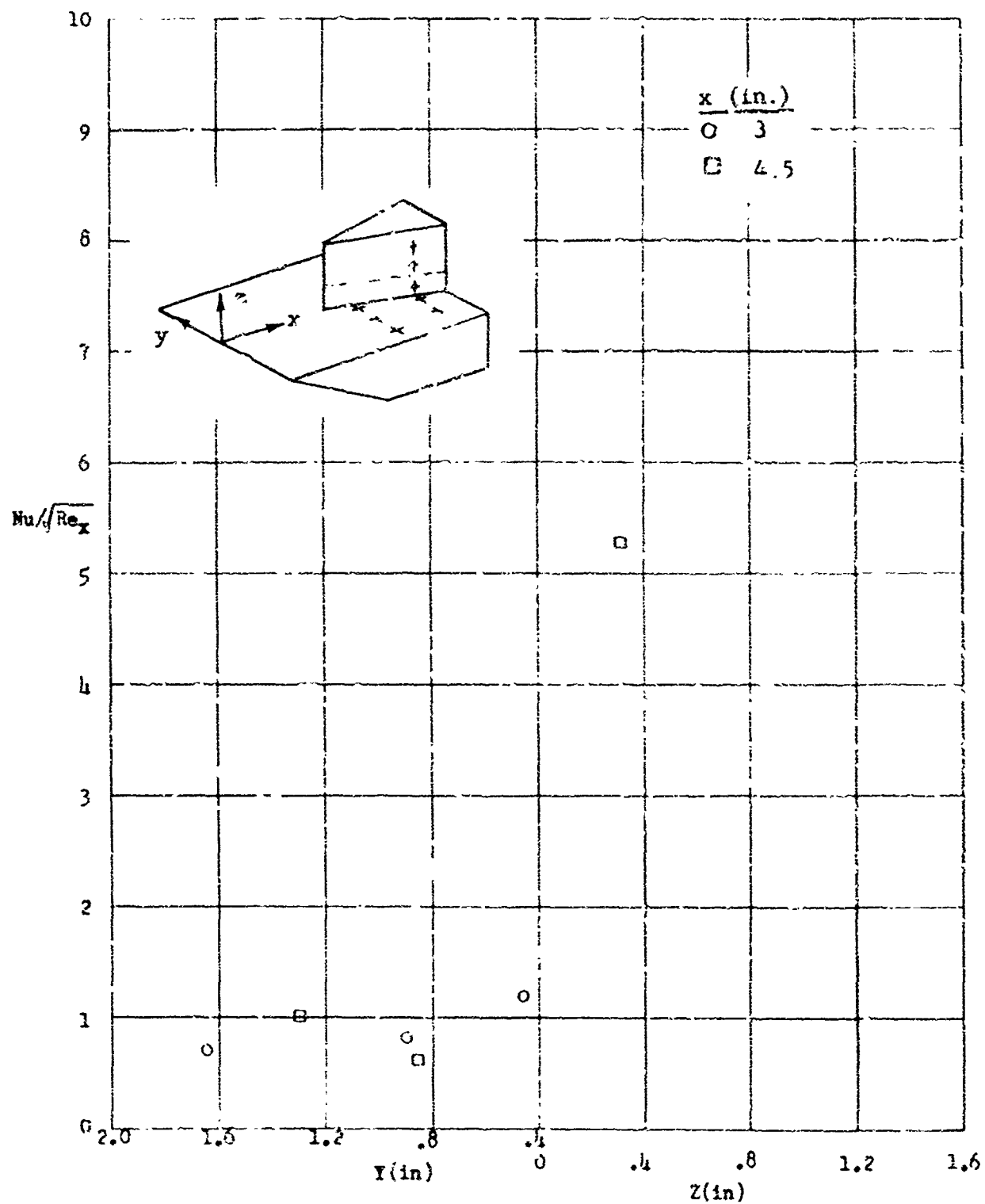Fig. 23  Wedge Plate Interaction Pressure Data, Small, Sharp LE Wedge, $M_\infty = 19$, $\alpha = 0$
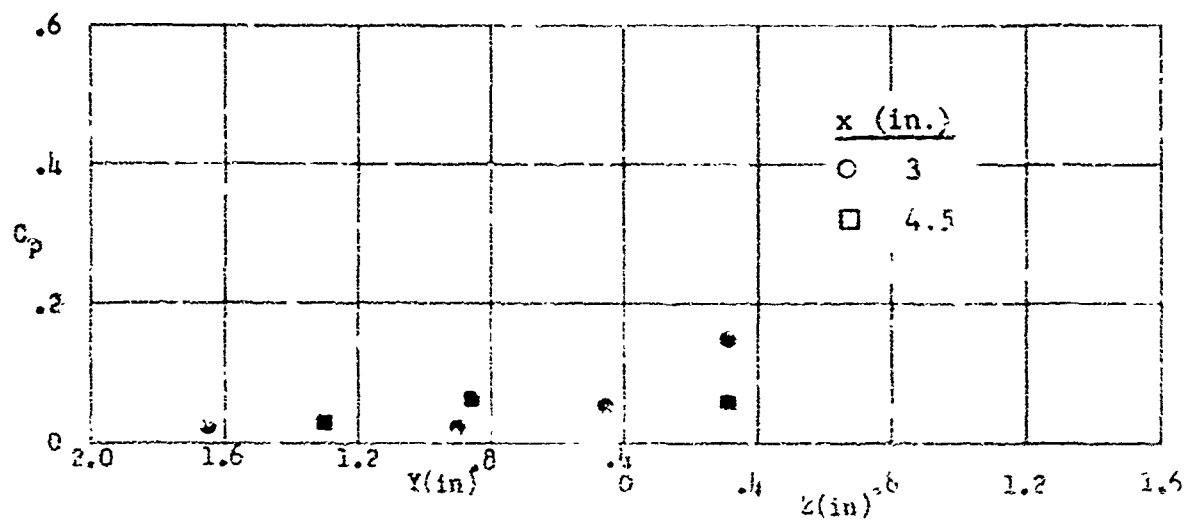


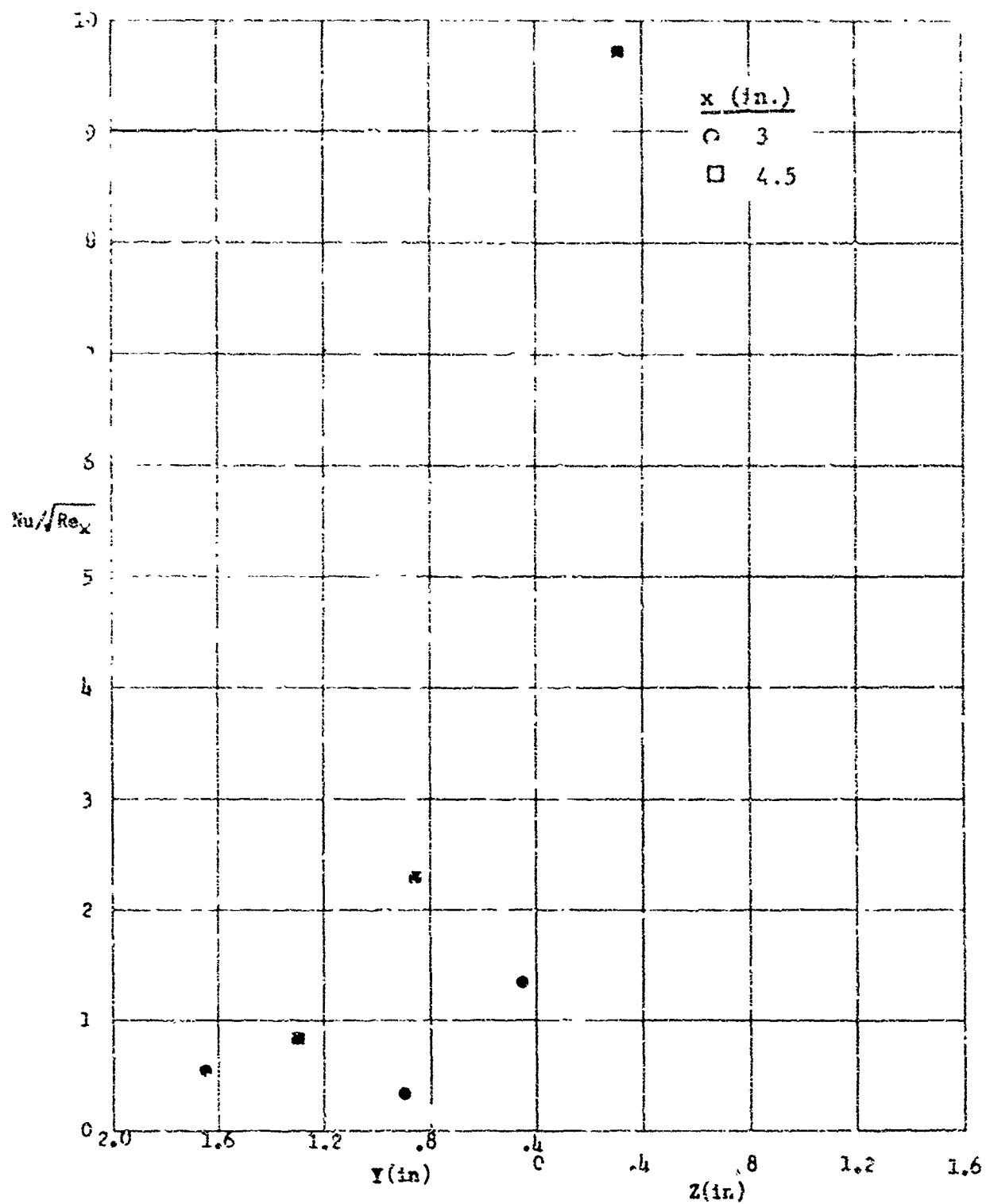Fig. 24  Wedge Plate Interaction Pressure Data, Small, Sharp LE Wedge, $M_\infty = 13$, $\alpha = 0$

34
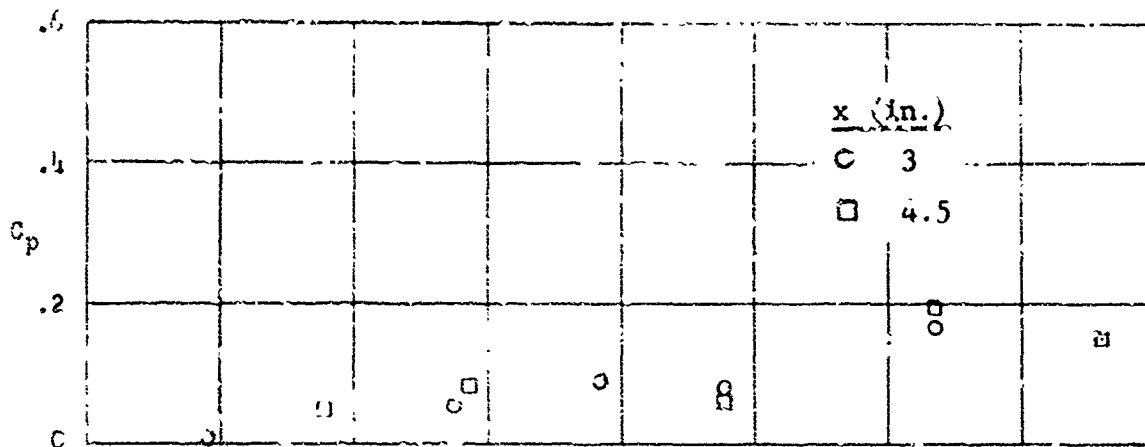
Fig. 25  Wedge Plate Interaction Pressure Data, Large, Sharp LE Wedge, $M_\infty = 19$, $\alpha = 0$
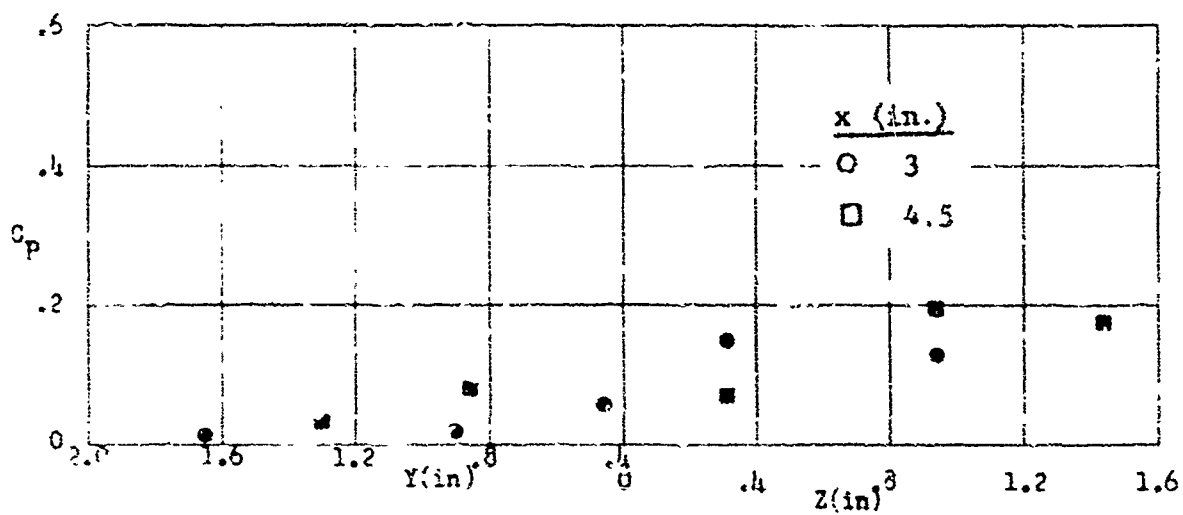


Fig. 26  Wedge Plate Interaction Pressure Data, Large, Sharp LE Wedge, $M_\infty = 13$, $\alpha = 0$

Fig. 27 Wedge Plate Interaction Heat Transfer Data, Small, Sharp LE Wedge, $M_\infty = 19$, $\alpha = 0$

Fig. 28 Wedge Plate Interaction Heat Transfer Data, Small, Sharp LE Wedge, $M_\infty = 13$, $\alpha = 0$
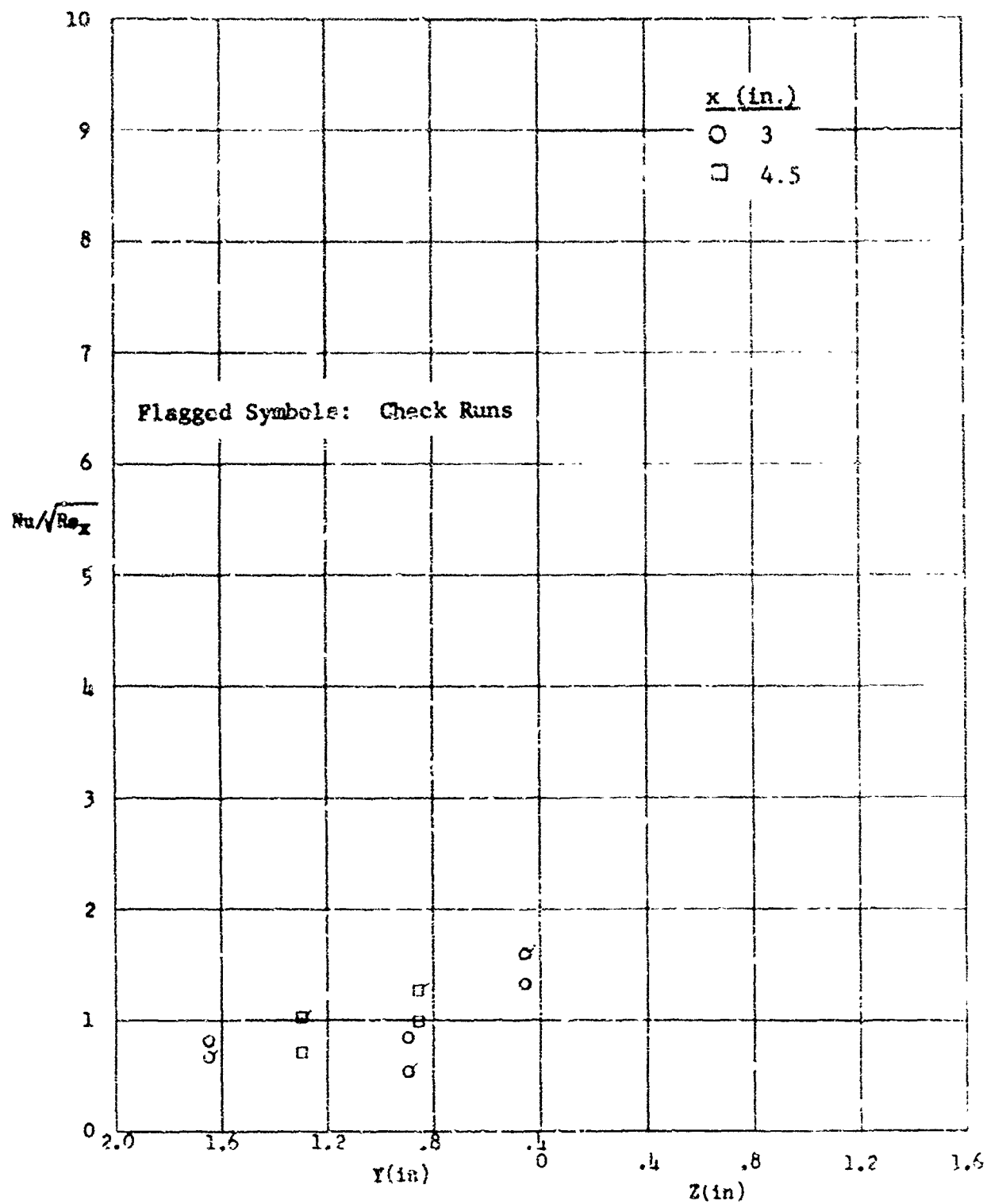
37

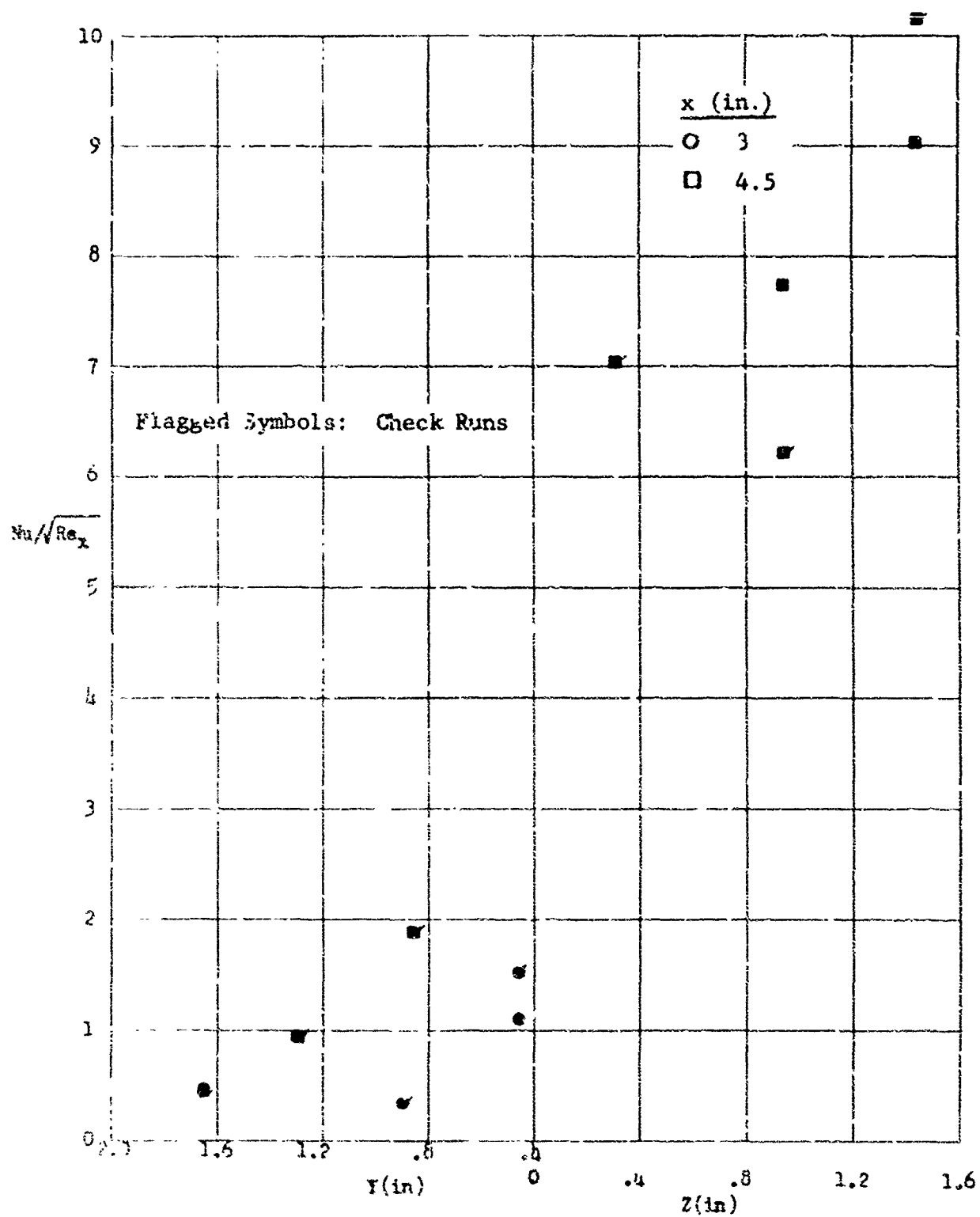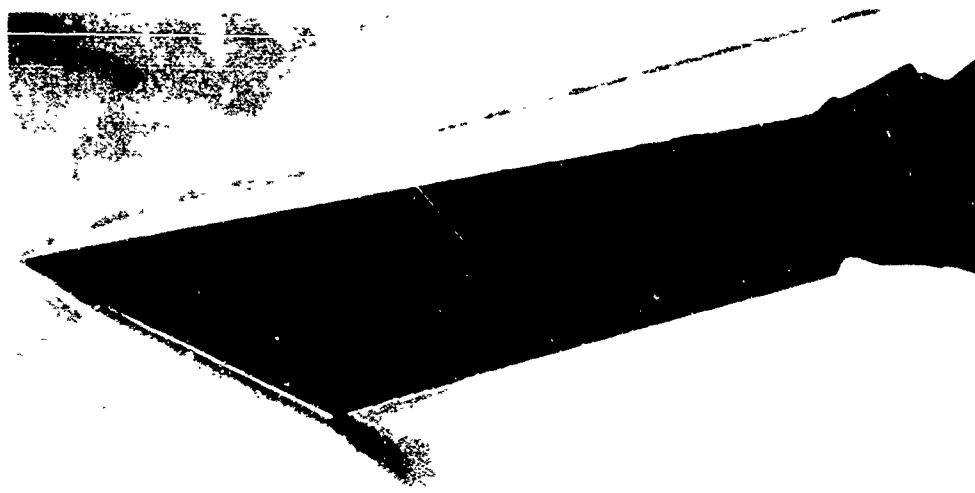Fig. 29  Wedge Plate Interaction Heat Transfer Data, Large, Sharp LE Wedge, $M_\infty = 19$, $\alpha \approx 0$

Fig. 30 Wedge Plate Interaction Heat Transfer Data, Large, Sharp LE Wedge, $M_\infty = 13$, $\alpha = 0$

Fig. 31 Schlieren Photograph Showing Model A at Mach 13, $\alpha = +10°$, $\delta = 0$, and Re/ft = 1.2 x $10^5$



Fig. 32 Schlieren Photograph Showing Model A at Mach 19, $\alpha = +30°$, $\delta = 15°$, and Re/ft = 0.8 x $10^5$

Fig. 33  Schlieren Photograph Showing Model A at Mach 19, $\alpha = 0$,
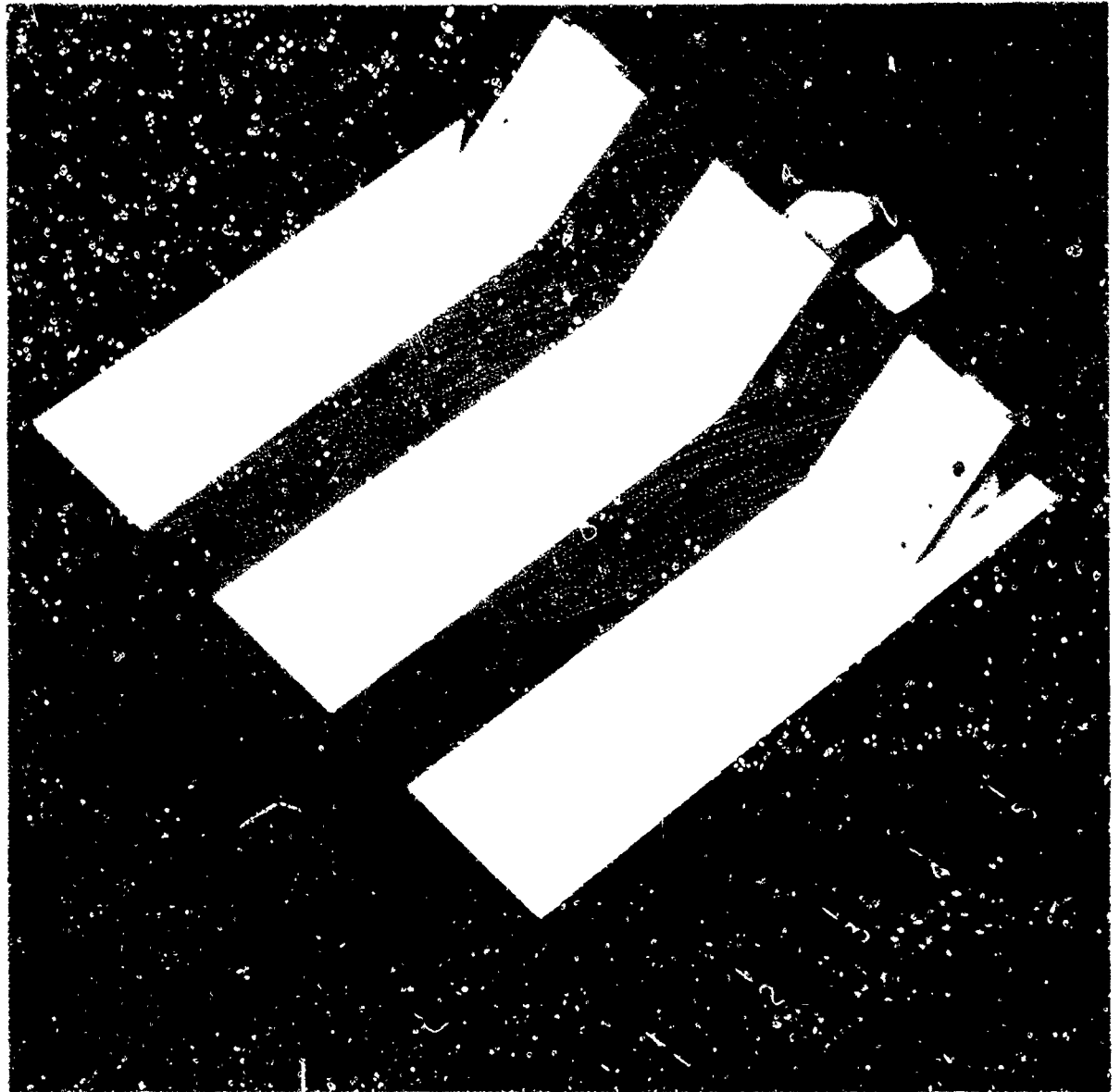$\delta = 45°$, and Re/ft $= 1.3 \times 10^5$

Fig. 34  Experiment with Krylon White:  Model A,  $\varepsilon = 45°$, Before Run

42
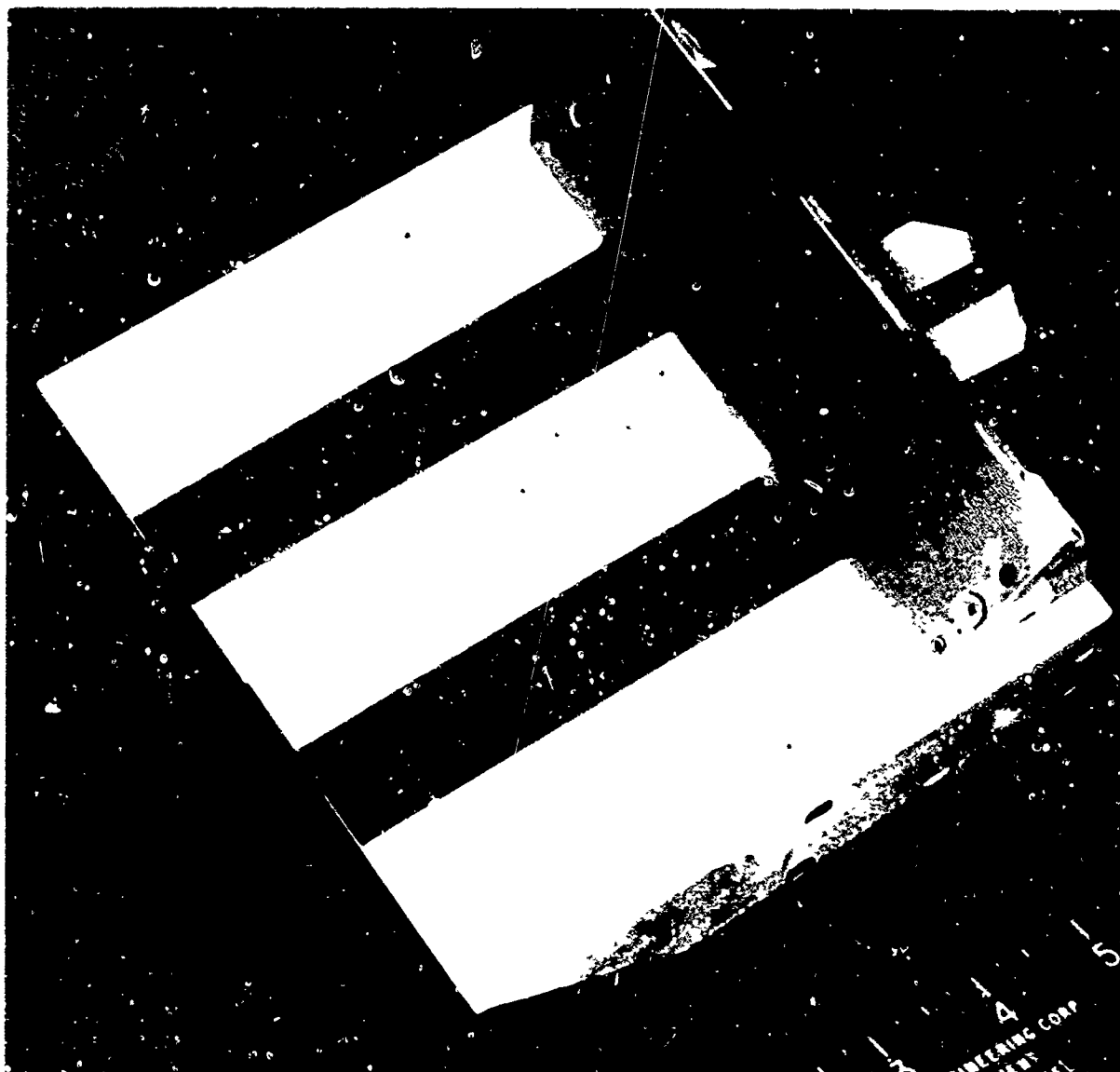
Fig. 35  Experiment with Krylon White:  Model A,  $\alpha = 0$, $\delta = 45°$, $M_\infty = 19$, and $Re_\infty/ft = 0.8 \times 10^5$
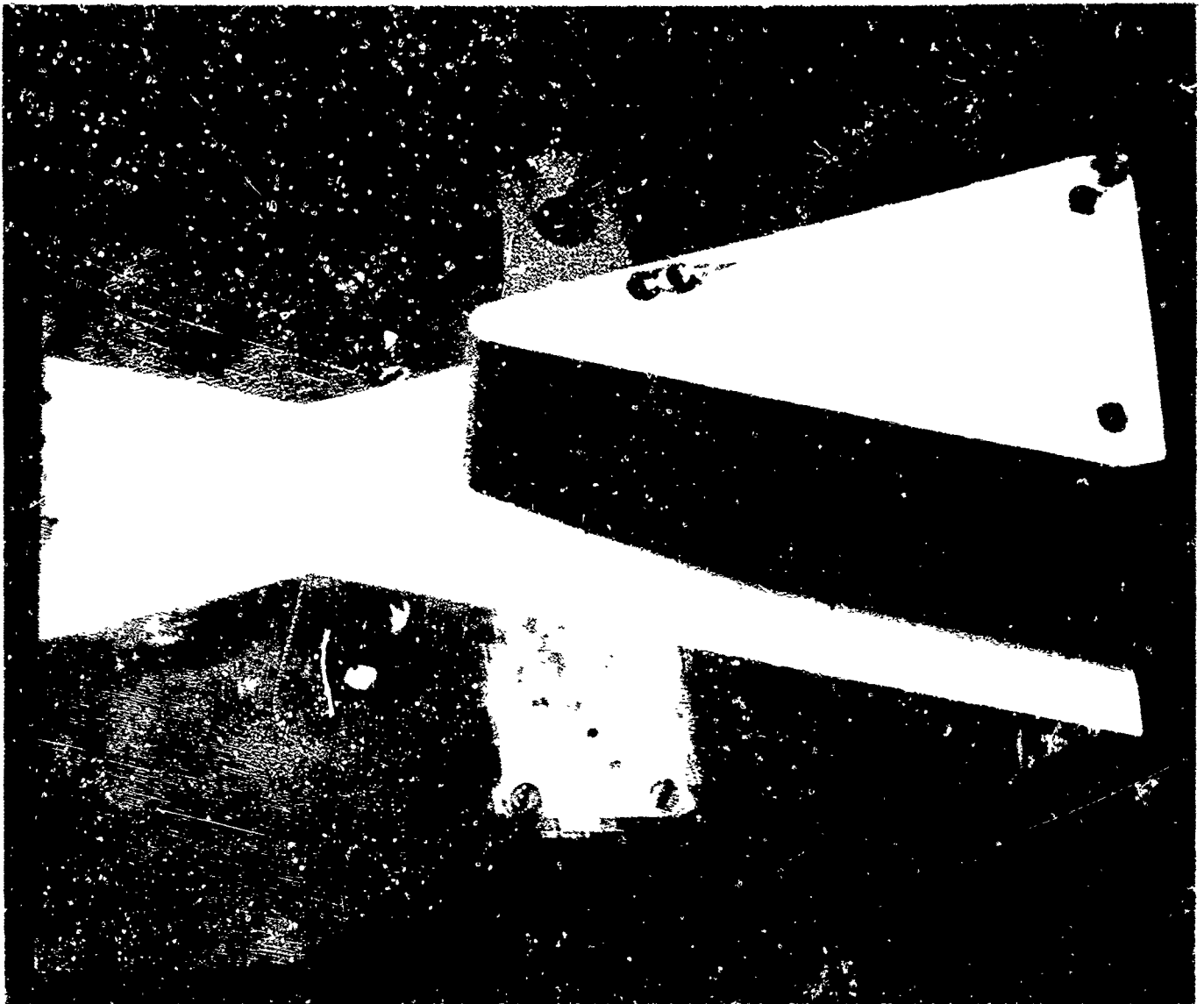
Fig. 36 Experiment with Krylon White:  Model B, Large, Blunt LE Wedge, $\alpha = 0$, $M_\infty = 13$, and Re/ft = 0.3 x $10^5$

ERRATA - December 1964

Due to printing defects, Figs. 31, 32, and 33 were
rendered without the flow detail that was present in the
original schlieren photographs.  To make these figures
meaningful, a new printing was made and is submitted herewith.

Air Force Flight Dynamics Laboratory
Research and Technology Division
Air Force Systems Command
Wright-Patterson Air Force Base, Ohio

Fig. 31  Schlieren Photograph Showing Model A at Mach 13, $\alpha = +10°$, $\delta = 0$, and Re/ft $= 1.2 \times 10^5$



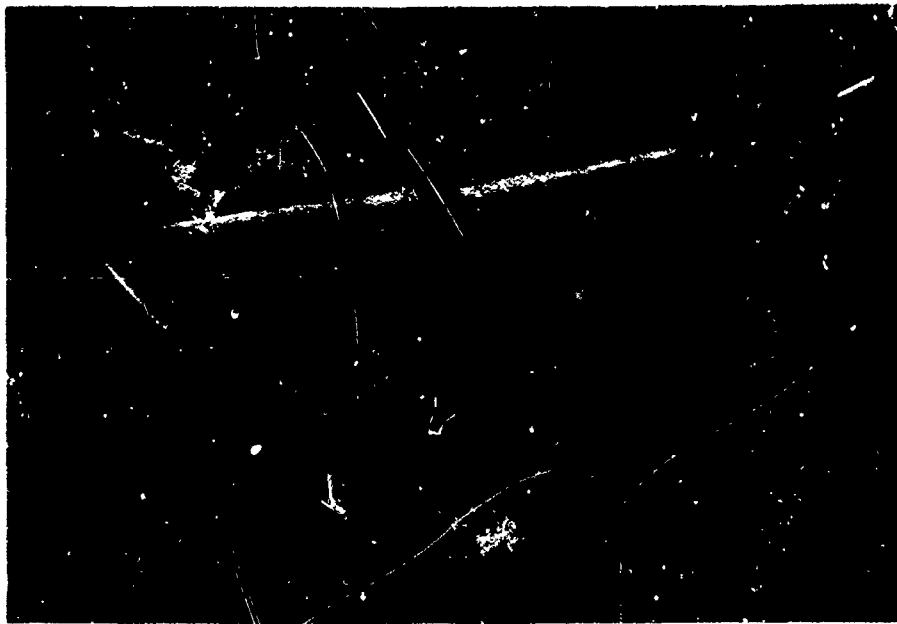Fig. 32  Schlieren Photograph Showing Model A at Mach 19, $\alpha = +30°$, $\delta = 15°$, and Re/ft $= 0.8 \times 10^5$

Fig. 33 Schlieren Photograph Showing Model A at Mach 19, $\alpha = 0$, $\delta = 45°$, and Re/ft = 1.3 x 10$^5$

ERRATA - December 1964

Due to printing defects, Figs. 31, 32, and 33 were
rendered without the flow detail that was present in the
original schlieren photographs. To make these figures
meaningful, a new printing was made and is submitted herewith.


Air Force Flight Dynamics Laboratory
Research and Technology Division
Air Force Systems Command
Wright-Patterson Air Force Base, Ohio

Fig. 31 Schlieren Photograph Showing Model A at Mach 13, $\alpha$ = +10°, $\delta$ = 0, and Re/ft = 1.2 x $10^5$


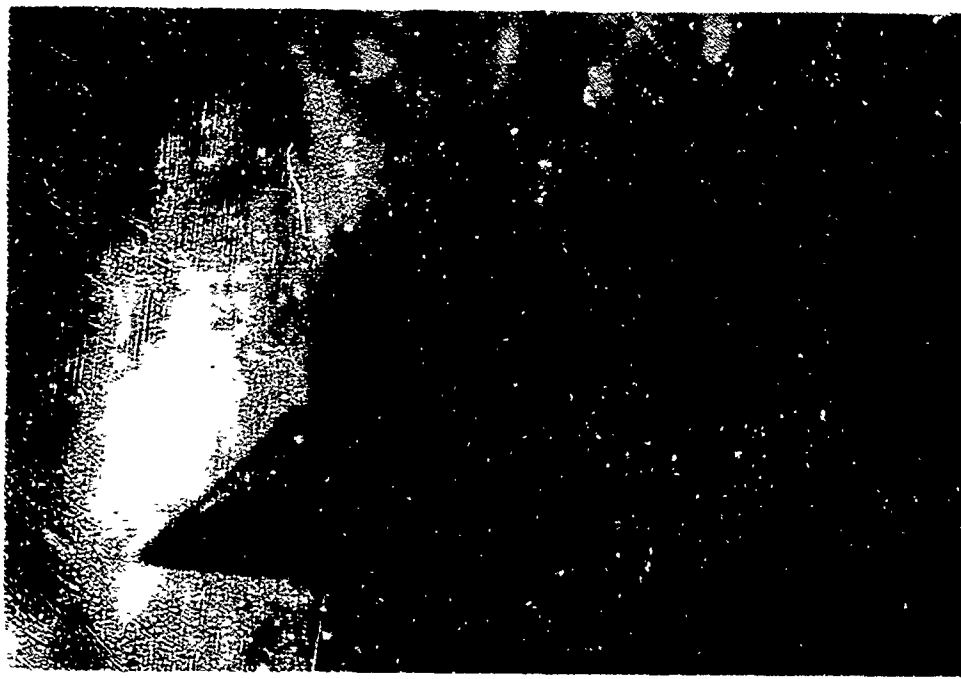
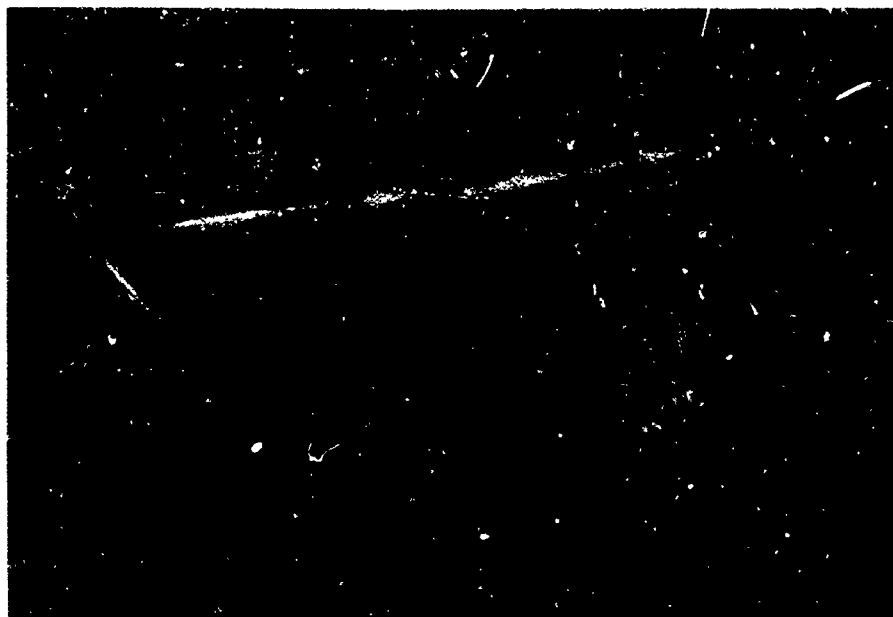Fig. 32 Schlieren Photograph Showing Model A at Mach 19, $\alpha$ = +30°, $\delta$ = 15°, and Re/ft = 0.8 x $10^5$

Fig. 33   Schlieren Photograph Showing Model A at Mach 19, $\alpha = 0$, $\delta = 45°$, and $Re/ft = 1.3 \times 10^5$